Published in final edited form as:

Nature. 2020 July ; 583(7815): 303–309. doi:10.1038/s41586-020-2446-y.

Systematic Quantitative Analysis of Ribosome Inventory Upon Nutrient Stress

Heeseon An[1,#], **Alban Ordureau**[1,#], **Maria Schultz**[1,2], **Joao A. Paulo**[1], **J. Wade Harper**[1,*]

[1]Department of Cell Biology, Blavatnik Institute of Harvard Medical School, Boston MA, USA

[2]Current Address: Department of Biochemistry, University of Würzburg, Würzburg, Germany

SUMMARY

Mammalian cells reorganize their proteomes in response to nutrient stress via translational suppression and degradative mechanisms using the proteasome and autophagy systems[1,2]. Ribosomes are central targets of this response, as they are responsible for translation and subject to lysosomal turnover upon nutrient stress[3–5]. Ribosomal (r)-protein abundance (~6% of the proteome, ~10^7 copies/cell)[6,7] and their enrichment in arginine (Arg) and lysine (Lys) residues has led to the hypothesis that they are selectively used as a source of basic AAs during nutrient stress via autophagy[4]. However, the relative contributions of translational and degradative mechanisms to the control of r-protein abundance during acute stress responses is poorly understood, as is the extent to which r-proteins are employed to generate AAs when specific building blocks are limited[7]. Here, we integrate quantitative global translatome and degradome proteomics[8] with genetically encoded Ribo-Keima[5] and Ribo-Halo reporters to interrogate r-protein homeostasis with and without active autophagy. Upon acute nutrient stress, cells strongly suppress r-protein translation, but, remarkably, r-protein degradation occurs largely through non-autophagic pathways. Simultaneously, loss of r-protein abundance is compensated for by reduced dilution of pre-existing ribosomes and reduced cell volume, thereby maintaining ribosome density within single cells. Withdrawal of basic or hydrophobic AAs induces translational repression without

*Corresponding author: wade_harper@hms.harvard.edu.
#These authors contributed equally to this work.

AUTHOR CONTRIBUTIONS

This study was conceived by H.A., A.O., and J.W.H. H.A., A.O., and M.S. performed all experiments. J.A.P. provided mass spectrometry expertise. The paper was written by H.A., A.O., and J.W.H.

COMPETING INTEREST STATEMENT

The authors declare the following competing interests: J.W.H. is a founder and consultant for Caraway Therapeutics and a consultant for X-Chem, Inc.

DATA AVAILABILITY

All the mass spectrometry proteomics data have been deposited to the ProteomeXchange Consortium via the PRIDE repository (http://www.proteomexchange.org/): Source Data Set 1 related to Supplementary Table 1 (PXD017852, PXD017853); Source Data Set 2 related to Supplementary Table 2 (PXD018252); Source Data Set 3 related to Supplementary Table 3 (PXD017857, PXD018158); Source Data Set 4 related to Supplementary Table 4 (PXD017856, PXD017855); Source Data Set 5 related to Supplementary Table 5 (PXD017858, PXD017851); Source Data Set 6 related to Supplementary Table 6 (PXD017861, PXD017860, PXD017859). Source data for all proteomics-based plots are provided in Supplementary Tables 1–6. Source data for all other plots are provided in the corresponding source data files. Gel source data for immunoblots are provided in Supplementary Fig. 1. All datasets generated within this study are available online, whereas the reagents are available from the corresponding author upon request.

Code availability

No custom software was developed for the analysis performed here.

differential induction of ribophagy, indicating that ribophagy is not used to selectively produce basic amino acids during acute nutrient stress. We present a quantitative framework describing the contributions of biosynthetic and degradative mechanisms to r-protein abundance and proteome remodeling during nutrient stress.

r-protein stoichiometry is controlled via both translation/assembly mechanisms and degradation of supernumerary r-proteins via the proteasome[9–11], while autophagy may facilitate *en mass* ribosome turnover[7,5]. Previous studies examining the effect of AA withdrawal or mTOR inhibition on r-protein homeostasis in mammalian cells have primarily focused on autophagic r-protein turnover, employing either immunoblotting to measure r-protein abundance for specific subunits[4] or Ribo-Keima to measure autophagic flux[5]. However, a global view of how cells regulate net ribosome balance upon nutrient stress is lacking, as r-protein degradation via autophagy represents only one component of the ribosome homeostasis system. To decode r-protein control mechanisms during nutrient stress, we developed a quantitative framework for analysis of r-protein abundance, synthesis, turnover, and subcellular partitioning using methods applicable to ensemble or single cell measurements (Extended Data Fig. 1a).

We initially examined the net balance of r-proteins upon acute AA withdrawal or inhibition of mTOR with a small molecule inhibitor Torin1 (Tor1) using quantitative proteomics (Fig. 1a–e, Extended Data Fig. 1b–d). HEK293 (293) and HCT116 cells with or without ATG8-conjugation (ATG5) or signaling (RB1CC1, also called FIP200) arms of the autophagy system were subjected to AA withdrawal or Tor1 treatment for 10 or 24h followed by 11-plex tandem mass tagging (TMT)-based proteomics (Fig 1b). We also mined our published dataset using 293T WT, ATG7$^{-/-}$, and RB1CC1$^{-/-}$ cells subjected to the same experimental pipeline[12] (Fig. 1c, Extended Data Fig. 1b). As expected, both treatments resulted in reduced levels of autophagy cargo receptors (GABARAPL2, LC3B, SQSTM1, TEX264) and endoplasmic reticulum proteins, dependent on ATG5/7 and RB1CC1[12] (Extended Data Fig. 1b–e and Table S1). In contrast, plots of the Log_2 ratio versus $-Log_{10}$ p-value for ≥70 of 80 r-proteins reveal only a modest (4.6–11.6%) reduction of r-protein levels with both forms of nutrient stress that was largely independent of autophagy (Fig. 1c–f, Extended Data Fig. 1b–d), although variation in the extent of decrease across individual r-proteins was observed (Fig. 1g, Extended Data Fig. 1f). This reduction in abundance for several r-proteins was not observable using quantitative immunoblotting (Extended Data Fig. 1g–k).

r-protein analysis with Ribo-Halo

The absence of obvious autophagy-dependent r-protein loss by proteomics with normalization based on total protein input created a paradox, given ribophagic flux with similar treatments using Ribo-Keima reporters[5]. Changes in r-protein abundance could reflect multiple mechanisms, including translational inhibition, degradation, or effects on ribosome dilution due to reduced cell division (Fig. 2a). To simultaneously examine new r-protein synthesis, the fate of pre-existing r-proteins, and dilution via cell division, we fused a Halo cassette with the surface-exposed C-termini of endogenous RPS3 and RPL29 genes in HCT116, 293T, or 293 cells (Extended Data Fig. 2a,b). Halo-fused proteins can be

covalently labeled in a temporally controlled manner using distinct fluorescent ligands, facilitating analysis of single cells by flow cytometry or imaging, and ensembles of cells using in-gel fluorescence. Halo-tagging did not affect r-protein abundance, translation rates, or the response to nutrient stress (Extended Data Fig. 2c,d). We also optimized concentrations, wash conditions, and compensation protocols to ensure complete Halo labeling with individual red (TMR) or green (R110) fluorescent ligands (Extended Data Fig. 2e–i, see Methods).

We initially measured the effect of mTOR inhibition (14h) on total RPS3-Halo and RPL29-Halo abundance in single HCT116 cells by flow cytometry using an 1h pulse labeling with cell-permeable red Halo ligand (Fig. 2b). The mean fluorescence/cell was reduced by ~25% with both cell lines upon Tor1 treatment (Fig. 2c,d). In parallel, we found that Tor1 treatment reduced cell diameter by ~10% (~25% reduction in volume), as noted previously[13], as well as reduced rates of cell division, thereby maintaining RPS3 and RPL29 density in single cells (Extended Data Fig. 2j,k). Thus, changes in cell number and cell size likely underlie the discrepancy between effects of nutrient stress measured by Ribo-Halo versus total proteomics, since the latter method employs normalized total protein input.

To simultaneously measure dilution of pre-existing r-proteins and new r-protein synthesis, HCT116 Ribo-Halo cells were treated for 1h with red Halo ligand to irreversibly label pre-existing r-proteins, free ligand rapidly washed out, and cells then incubated in rich media with green Halo ligand for 8, 16 or 24h to label newly translated r-proteins (Fig. 2e, Extended Data Fig. 2l). As expected, the relative contribution of pre-existing RPS3 and RPL29 to the entire pool of these proteins in single cells decreased with time, representing dilution by cell division (Fig. 2e, Extended Data Fig. 2l). Fifty % of pre-existing r-proteins were observed at ~16h, consistent with cell proliferation rates measured independently (Extended Data Fig. 2k). The total r-protein abundance/cell was maintained via synthesis of new r-proteins labeled with green Halo ligand, consistent with a doubling in ribosome number during one cell cycle. Upon inhibition of mTOR during labeling with green Halo ligand (Fig. 2f, Extended Data Fig. 2m), we observed reduced dilution of pre-existing r-proteins at 8, 16, and 24h in parallel with reduced cell division, and a reduction in the production of newly synthesized (green) r-proteins, apparently reflecting translational inhibition. A reduction of total r-proteins (red + green) by 10–30% was consistent with single ligand labeling. Reduced new synthesis and dilution of pre-existing r-proteins was also observed via imaging or in-gel fluorescence in Ribo-Halo cells upon Tor1 treatment (14h) (Fig. 2g,h, Extended Data Fig. 2n–q). Consistent with residual mTOR activity in HCT116 relative to 293T cells, we observed differential repression of new RPS3-Halo synthesis by pulse-chase Halo labeling (40% versus 60%) (Extended Data Fig. 2o,r). Critically, r-protein abundance, dilution, new synthesis, or cell size changes upon mTOR inhibition (14 or 24h) were unaltered in cells lacking ATG7 or RB1CC1 (Extended Data Fig. 3a–n). Thus, the overall abundance of r-proteins in response to mTOR inhibition reflects reduced new r-protein synthesis and reduced dilution of pre-existing r-proteins, the magnitude of which may vary with cell type. Autophagic turnover of r-proteins and rRNA is unlikely to provide a mechanism to reverse translation suppression and cell growth under acute conditions.

Translatomics upon nutrient stress

We next developed a quantitative translatome approach to systematically examine r-protein synthesis during nutrient stress by employing azidohomoalanine (AHA) metabolic labeling (Fig. 3a,b). AHA activation by $tRNA^{Met}$-synthetase allows incorporation of azides into proteins[14] that can then be functionalized through click chemistry,[8] thereby allowing measurement of ongoing translation using TMR alkyne for in-gel quantification or biotin alkyne for purification with streptavidin resin and TMT-based proteomics (Fig. 3b). We optimized AHA labeling (250 μM) to minimize effects on mTOR activity while allowing sufficient AHA incorporation (Extended Data Fig. 4a–g, and METHODS). As expected based on ribosome profiling and ^{35}S-Cys/Met incorporation[1], overall translation was reduced by 60–70% upon mTOR inhibition or AA withdrawal (3h) as measured by TMR labeling (Fig. 3c, Extended Data Fig. 4h). We then quantified translation of >8,200 proteins by AHA-TMT proteomics. The vast majority of proteins were translationally repressed upon mTOR inhibition or AA withdrawal (3h), a notable exception being eIF4EBP1 with mTOR inhibition[2,15] (Fig. 3d,e; Extended Data Fig. 4i). Interestingly, the majority of r-proteins were translationally repressed beyond the median value, consistent with 5' terminal oligopyrimidine (TOP) motifs in their mRNAs[1]. mTOR inhibition more selectively repressed r-protein translation than AA withdrawal, despite similar levels of proteome-wide translation suppression (Extended Data Fig. 4h,j). In addition, we identified proteins whose translation was more selectively suppressed (Group 1), largely unchanged (Group 2), or differentially affected by the two treatments (Groups 3 and 4) (Extended Data Fig. 4k–o). Surprisingly, the extent of translational suppression in ATG7$^{-/-}$ and RB1CC1$^{-/-}$ 293T cells was comparable to WT cells (Fig. 3e; Extended Data Fig. 4p–r). Thus, global translational suppression of r-proteins contributes to ribosome abundance control during acute nutrient stress, and this is not appreciably affected by the cells ability to recycle AAs through autophagy under acute conditions. Lastly, variation in the extent of translational suppression across individual r-proteins was observed (Extended Data Fig. 4s).

Global degradomics upon nutrient stress

To directly examine r-protein degradation during nutrient stress and the contribution of autophagy to turnover (Fig. 3f), we pulse labeled WT, ATG7$^{-/-}$, and RB1CC1$^{-/-}$ 293T cells with AHA, allowed 1h for turnover of short-lived proteins in rich media, and then compared the abundance of biotinylated AHA-labeled proteins with or without mTOR inhibition (12h) by TMT proteomics (Fig. 3g; Extended Data Fig. 5a,b). From >8300 proteins quantified, we found 3 patterns of turnover (Fig. 3h; Extended Data Fig. 5c,d): 1) Pattern 1 with autophagy-dependent degradation, including several autophagy receptors[16], 2) Pattern 2 with autophagy-independent turnover that is enhanced by mTOR inhibition, including several proteins known to be degraded by the proteasome upon mTOR inhibition[17], and 3) Pattern 3 proteins with autophagy-independent stabilization upon mTOR inhibition. Interestingly, r-proteins conformed to Pattern 2, and were degraded in a largely autophagy-independent manner, although degradation rates varied for individual r-proteins with a correlated rank order with or without Tor1 (R^2~0.7) (Fig. 3i,j; Extended Data Fig. 5e,f). As expected[12], 326 ER proteins were degraded in an autophagy-dependent manner and serve as a positive control for this degradomics approach to detect autophagy substrates (Extended Data Fig.

5g–i). To confirm these results, we performed a time-course experiment examining global degradomics at 5, 10, and 15h post-mTOR inhibition (Extended Data Fig. 6a–g). Consistently, mTOR inhibition induced accelerated r-protein turnover in a time-dependent manner, which was largely independent of an active autophagy pathway.

Proteome partitioning upon AA stress

Given that several ribosome assembly steps occur in the nucleus/nucleolus, we examined whether nutrient stress alters the nuclear to cytosolic ratio of r-protein (Extended Data Fig. 7a). After optimizing isolation of nuclei and cytosol (Extended Data Fig. 7b–f), we quantified cytosolic and nuclear protein and phosphoprotein pools with or without AA withdrawal (3h) (Extended Data Fig. 7g–l). We observed decreased FOXK1 nuclear abundance, decreased RPS6, FOXK1/2, CAD phosphorylation, and increased TFEB, MITF, and TFE3 nuclear abundance, indicating mTOR inhibition[18] (Extended Data Fig. 7j–m). We also uncovered several nucleolar ribosome biogenesis factors (PWP1, SDAD1, and NVL)[19] that accumulate in the cytosol upon AA withdrawal (Extended Data Fig. 7j,k,n–p). In contrast, r-protein distribution was largely unchanged after AA withdrawal. As expected, ~91% of 60S r-proteins and 95% of 40S r-proteins are cytoplasmic in untreated cells, consistent with the longer time required to assemble the 60S subunit at steady-state and the larger fraction of 40S subunits that are assembled in the cytosol[20] (Extended Data Fig. 8a). Upon AA withdrawal, the nuclear r-protein pool was reduced by 20% (~1.5% of the total ribosome pool) (Extended Data Fig. 8b–d), indicating that r-protein redistribution plays a very minor role in ribosome homeostasis under these conditions.

Ribophagic flux during nutrient stress

Our finding that cells lacking autophagy have no obvious defects in the response to nutrient stress based on total proteome, Ribo-Halo, translatome, and degradome analysis led us to further quantify ribophagic flux. Using Ribo-Keima reporters[5], we estimated that 3–4% of ribosomes are degraded in the lysosome after Tor1 treatment (10h) (Extended Data Fig. 8e–h), consistent with prior studies[5]. The magnitude of autophagic flux is such that RPS3 turnover measured via AHA-TMT proteomics, which is ~20% (SD < 0.1) in 12h, is not obviously sensitive to the deletion of ATG7 or RB1CC1 (Extended Data Fig. 8i). NUFIP1, a subunit of the nucleoplasmic R2TP pathway involved in 60S rRNA biogenesis[21], was reported to traffic to the cytosol in response to nutrient stress and to function as a selective ribophagy receptor for lysosomal delivery[4,22]. The absence of NUFIP1 re-localization upon AA withdrawal by TMT proteomics (Extended Data Fig. 7j,k) led us to re-evaluate its role in ribophagy. First, NUFIP1$^{-/-}$ 293T cells display reduced r-protein levels in rich media, consistent with the previously defined role for R2TP in 60S biogenesis (Extended Data Fig. 9a,b). Second, NUFIP1 deletion had no effect on either total Ribo-Halo abundance and synthesis/dilution (Extended Data Fig. 9c–e) or on r-protein abundance as measured by TMT proteomics (Extended Data Fig. 9f–i) during mTOR inhibition. Third, RPS3-Keima flux was unaffected in NUFIP1$^{-/-}$ cells undergoing nutrient stress (Extended Data Fig. 9j). We conclude that NUFIP1 is not required for ribophagic flux under these stress conditions.

Single AA or purine depletion

The ~2-fold enrichment of basic AAs in r-proteins relative to the proteome together with the fact that ribosomes are rich in rRNA has led to the hypothesis that ribosomes may be selectively used for autophagy in response to decreased levels of these building blocks[4,23]. We employed our r-protein analysis pipeline to evaluate selective withdrawal of Arg, Lys, or Leu on ribosome homeostasis and ribophagic flux (Fig. 4a). When compared with Tor1 or AA withdrawal, Leu and Arg withdrawal resulted in only a partial loss of mTOR activity (Extended Data Fig. 10a,b), as found previously[24]. However, Arg withdrawal promoted stronger translational inhibition, as measured by puromycin incorporation assay (Extended Data Fig. 10b,c), two-color RPS3-Halo assay (Fig. 4b; Extended Data Fig. 10d), and translatome analysis (Fig. 4c,d; Extended Data Fig. 10e–h). The order of translational suppression was Arg≥Tor1>Lys>Leu for both the total proteome and r-proteins. However, ribophagic flux[5] was <3.4% in all cases (Extended Data Fig. 10i), indicating that acute loss of basic AAs does not selectively promote ribophagy.

We also found that 6-mercaptopurine (6-MP), an inhibitor of HPRT1 (hypoxanthine phosphoribosyltransferase 1) that blocks production of GMP and IMP[25] (Extended Data Fig. 11a), dramatically suppressed proteome and r-protein translation (Extended Data Fig. 11b–d), and also suppressed both dilution and new synthesis in the two-color Ribo-Halo assay (Extended Data Fig. 11e,f). However, the reduction in r-protein abundance measured by TMT-proteomics was ATG5-independent (Extended Data Fig. 11g). Consistent with this, ribophagic flux as measured using the RPS3-Keima processing assay was not detectably induced during 6-MP treatment (24h) in stark contrast to arsenite treatment[5] (Extended Data Fig. 11h), indicating that autophagy is unlikely to be a major driver in regulation of r-protein abundance in response to inhibition of purine biosynthesis.

Framework for r-protein homeostasis

Here, we develop an experimental pipeline for broadly probing the integration of biosynthetic and degradative mechanisms controlling signal-dependent proteome remodeling with a focus on r-proteins. The major contributors to r-protein abundance control with either mTOR inhibition or AA withdrawal were: 1) translation suppression of r-proteins, 2) reduced dilution of pre-existing ribosomes reflecting prolonged cell proliferation rates, and 3) non-autophagic r-protein degradation (Fig. 4e). In contrast, ribophagy represented a relatively small contribution to overall changes in ribosome abundance (3~4% in 10–12h). The finding that r-protein turnover parallels proteasomal targets by degradomics (Pattern 2, Fig. 3h) suggests proteasome involvement, but relevant ubiquitin ligases[7] remain unknown.

We developed a quantitative framework (Fig. 4e, Extended Data Fig. 11i,j) which facilitates an understanding of the factors that contribute to the cellular concentration of ribosomes, taking into account ribosome number, cell division timing, and cell volume. A central element of the model is that ribosome abundance/cell increases by 2-fold over the course of the cell cycle and is re-set upon division. Under nutrient stress conditions, alterations in r-protein synthesis and degradation rates slow the increase in r-protein abundance (numerator), which is partially compensated for by changes in cell volume and the timing of division

(denominator) (Extended Data Fig. 11i,j). Incorporation of our translational inhibition, degradation, cell volume and division rate data into this model accurately estimates the total change in ribosome concentration measured by total proteomics. However, the current model uses zero order kinetics for changes in translation, turnover, and cell division, and more precise models will require measurements of rates of change during the stress interval. Our framework highlights the importance of considering multiple r-protein homeostasis mechanisms simultaneously to fully understand the similarities and differences across cell systems that may respond to nutrient stress in distinct ways. In this regard, ribophagy in budding yeast has been proposed to be a major contributor to proteome remodeling in response to nitrogen deficiency[3]. This apparent differential utilization of autophagy in yeast versus mammalian tissue culture cells could reflect the fact that r-protein abundance in yeast is an order of magnitude higher than that seen in mammalian cells, but is also complicated by the fact that the duration of nutrient stress applied (24h) is ~16 times the cell division time[7,26]. Interestingly, approximately 10% of ER proteins are degraded within 10h of AA withdrawal in human cells, and this is blocked by genetic ablation of autophagy[12] as verified here by degradomics (Extended Data Fig. 5g–i). Given that the contribution of ER proteins to total proteome mass rivals that of r-proteins[6,7], ER may constitute a major target for autophagic degradation in response to AA withdrawal or mTOR inhibition. Ribosomes may also be degraded to some extent by autophagy via association with rough ER, as visualized *in situ* by electron microscopy[27]. It seems likely that in vivo and with chronic nutrient stress, autophagy will be responsible for generation of AAs such as arginine, as has been shown in the context of tumorigenesis[28].

METHODS

Cell lines

HEK293 (human embryonic kidney, fetus, ATCC CRL-1573, RRID: CVCL_0045), HCT116 (human colorectal carcinoma, male, ATCC CCL-247, RRID: CVCL_0291), and HEK293T (human embryonic kidney, fetus, ATCC CCL-3216, RRID: CVCL_0063) cells were grown in Dulbecco's modified Eagle's medium (DMEM, high glucose and pyruvate) supplemented with 10% fetal calf serum and maintained in a 5% CO_2 incubator at 37°C.

Generation of RPS3-HaloTag7 and RPL29-HaloTag7 knock-in cell lines using CRISPR-Cas9 gene editing

gRNAs targeting C-terminus region of human *RPS3* and *RPL29* genes were designed using the CHOPCHOP website (http://chopchop.cbu.uib.no/). The guide sequences for *RPS3* gene (5'- GACATACCTGTTATGCTGTGTTT-3') or *RPL29* gene (5'-GAGATATCTCTGCCAACATG-3') were assembled into pX459 plasmid[29]. Donor vectors were constructed by assembling HaloTag7 transgene with upstream and downstream homology arms (650 nucleotide each) into digested pSMART plasmid by Gibson assembly. HEK293, HEK293T, and HCT116 cells were transfected with donor and gRNA vectors (1 to 1 ratio) by Lipofectamine 3000 (Invitrogen). Five days after the transfection, the pool of transfected cells was treated with 100 nM Halo-TMR ligand for 1h, followed by three times of washing. Fluorescence positive cells were sorted into 96 well plates by flow-cytometry (MoFlo Astrios EQ, Beckman Coulter). Three weeks later, the expanded single-cell colonies

were screened for the integration of the HaloTag7 transgene by immunoblotting with α-RPS3 or α-RPL29, followed by genotyping.

Generation of gene knock-out cell lines using CRISPR-Cas9 gene editing

RB1CC1, ATG5, *ATG7, and NUFIP1* knock-out on 293T, 293, and HCT116 cell lines was carried out by plasmid-based transfection of Cas9/gRNA using pX459 plasmid as described[29]. Initially, six gRNAs for *ATG5*, *ATG7*, and *NUFIP1* and four guide RNAs for *RB1CC1* knock-out were designed using CHOPCHOP website. Puromycin selection was followed 24 hours after the transfection. 48 hours after the transfection, gene cleavage efficiency of each guide RNA was measured by Surveyor assay. The following gRNA was shown the best cutting efficiency among the tested guides: 5'-GTCCAAGGCACTACTAAAAG-3' (exon2) for *ATG7,* 5'-GATCACAAGCAACTCTGGAT-3' (exon5) for *ATG5*, 5'-GAAGAATCTGGGCGTCGAAG-3' (exon1) for *NUFIP1*, and 5'-GCTACGATTGACACTAAAGA-3' (exon7) for *RB1CC1*,. Single cell was sorted into 96-well plate using limiting dilution method, and expanded clonal cells were screened by immunoblotting with α-ATG7, α-ATG5, α-RB1CC1, NUFIP1, and α-LC3B antibodies.

Reagents

Antibodies: RPS3 (Cell Signaling Technology, 9538); RPL28 (Abcam, ab138125), RPS15a (Bethyl Lab, A304–990A-T), ATG7 (Cell Signaling Technology, 8558S), Keima (MBL international, M182–3), LC3B (MBL international, M186–3), ATG5 (Cell Signaling Technology, 12994), p70 S6K phospho-T389 (Cell Signaling Technology, 9234S), phospho-S6 ribosomal protein Ser253, 236 (Cell Signaling Technology, 4858), TEX264 (Sigma, HPA017739), RPL23 (Bethyl Lab, A305–010A-T), RPL7 (Bethyl Lab, A300–741A-T), RPL29 (Proteintech Group, 15799–1-AP), Tubulin (Abcam, ab7291), SQSTM1 (Novus Biologicals, H00008878-M01), Anti-puromycin antibody (EMD millipore, MABE343), NUFIP1 (Proteintech Group, 12515–1-AP), RPS6 (Cell Signaling Technology, 2217), 4EBP1 (Cell Signal Technology, 9644), Lamin A/C (Cell Signal Technology, 4777), TFEB (Cell Signal Technology, 4042), SDAD1 (Bethyl Lab, A304–692A-T), NVL (Proteintech Group, 16970–1-AP), c-Maf (RnD systems, MAB8227-SP), IRDye® 800CW Streptavidin (LI-COR, 926–32230), IRDye 800CW Goat anti-Rabbit IgG H+L (LI-COR, 925–32211), IRDye 680 RD Goat anti-Mouse IgG H+L (LI-COR, 926–68070)

Chemicals, Peptides, and Recombinant Proteins: Torin1 (Cell Signal Technology, 14379), SAR405 (APExBio, A8883), Azidohomoalanine (Click Chemistry Tools, 1066–1000), 5-TAMRA alkyne (Click Chemistry Tools, 1255–1), Biotin-PEG4-Alkyne (Click Chemistry Tools, TA105–25), HaloTag® R110Direct™ Ligand (Promega, G3221), HaloTag TMR (5mM) (Promega, G8251), 6-Mercaptopurine monohydrate (Sigma, 852678–1G-A), Sodium ascorbate (VWR international, 95035–692), Poly-L-lysine solution (Sigma, P4832), FluoroBrite DMEM (Thermo Fisher Scientific A, 1896701), Benzonase Nuclease HC (Millipore, 71205–3), Urea (Sigma, Cat#U5378), SDS (Sodium Dodecyl Sulfate) (Bio-Rad, Cat#1610302), SURVEYOR Mutation Detection Kit (Integrated DNA Technologies, 706025), REVERT™ Total Protein Stain kit (LI-COR, P/N926–11010), 1,1,1,3,3,3-Hexafluoro-2-propanol (Sigma, 52517), Dulbecco's MEM (DMEM), high glucose, pyruvate

(Gibco / Invitrogen, 11995), Dulbecco's MEM (DMEM), Low Glucose, w/o Amino Acids (US Biological, D9800–13), TCEP (Gold Biotechnology), Puromycin (Gold Biotechnology, P-600–100), Formic Acid (Sigma-Aldrich, 94318), Protease inhibitor cocktail (Sigma-Aldrich, P8340), PhosSTOP (Sigma-Aldrich, 4906845001), Trypsin (Promega, V511C), Lys-C (Wako Chemicals, 129–02541), Rapigest SF Surfactant (Glixx Laboratories, Cat#GLXC-07089), EPPS (Sigma-Aldrich, Cat#E9502), 2-Chloroacetamide (Sigma-Aldrich, C0267), TMT 11plex Label Reagent (Thermo Fisher Scientific, Cat#90406 & #A34807), TMTpro 16plex Label Reagent (Thermo Fisher Scientific, Cat#A44520), Hydroxylamine solution (Sigma Cat#438227), Empore™ SPE Disks C18 (3M - Sigma-Aldrich Cat#66883-U), Sep-Pak C18 Cartridge (Waters Cat#WAT054960 and #WAT054925), SOLA HRP SPE Cartridge, 10 mg (Thermo Fisher Scientific, Cat#60109–001), High pH Reversed-Phase Peptide Fractionation Kit (Thermo Fisher Scientific, Cat#84868), High-Select Fe-NTA Phosphopeptide Enrichment Kit (Thermo Fisher Scientific, Cat#A32992), Bio-Rad Protein Assay Dye Reagent Concentrate (Bio-Rad,#5000006), Pierce Quantitative Colorimetric Peptide Assay (Thermo Fisher Scientific, #23275).

Amino acid free medium preparation (500 ml)

DMEM powder (4.16 g, US biological) and 1.85 g sodium bicarbonate were dissolved in 400 ml H_2O. To the solution, 1.75 g of glucose, 5 ml of 100x sodium pyruvate (final conc. = 1 mM) and 50 ml of dialyzed fetal calf serum were added. 150 μl of 6N HCl was slowly added to bring the pH to 7.4. The final volume was adjusted to 500 ml. The media was filtered through 0.2 μm filter and kept at 4 °C.

Single Amino acid (Met, Lys, Arg) free medium preparation (1 L)

Base-medium for the indicated amino acid withdrawal was prepared by dissolving DMEM powder (8.32g, US biological), 3.7 g/L sodium bicarbonate, and 3.5 g/L glucose, 30 mg/L glycine, 63 mg/L cystine 2HCl, 580 mg/L glutamine, 42 mg/L histidine HCl-H_2O, 105 mg/L isoleucine, 66 mg/L phenylalanine, 42 mg/L serine, 95 mg/L threonine, 16 mg/L tryptophan, 104 mg/L tyrosine 2Na $2H_2O$, 94 mg/L valine, and 105 mg/L leucine in 880 mL H_2O, and pH titrated to pH 7.2 using 2M HCl. The base-media was filtered through 0.2 μm filter and kept at 4 °C. Before each experiment, 0.9 equivalence (v/v) of the base-medium was added by 0.1 equivalence (v/v) of dialyzed bovine serum albumin, 0.01 equivalence (v/v) of 100 × sodium pyruvate (final conc. 1mM) and 0.001 equivalence of 1000 × amino acids (methionine stock: 37.5 mg/ml (final 37.5 mg/L = 250 μM), Lysine HCl stock: 146 mg/ml (final 146 mg/L), Arginine HCl stock: 84 mg/ml (final 84 mg/L) except the limiting amino acid.

Leucine free medium with or without Met preparation (1 L)

Solubility of Leucine in H_2O was too low to be added at the last step as a concentrate. Therefore, leucine free medium had to be prepared separately from the -Lys and -Arg medium. DMEM powder (8.32g, US biological), 3.7g/L sodium bicarbonate, and 3.5 g/L glucose, 30 mg/L glycine, 63 mg/L cystine 2HCl, 580 mg/L glutamine, 42 mg/L histidine HCl-H_2O, 105 mg/L isoleucine, 66 mg/L phenylalanine, 42 mg/L serine, 95 mg/L threonine, 16 mg/L tryptophan, 104 mg/L tyrosine 2Na $2H_2O$, 94 mg/L valine, 146 mg/L Lys, and 84

mg/L Arg were dissolved in 880 mL H_2O, and pH titrated to pH7.2 using 2M HCl. The base-media was filtered through 0.2 micron filter and kept at 4 °C. Before each experiment, 0.9 equivalence (v/v) of the base medium was added by 0.1 equivalence (v/v) of dialyzed bovine serum albumin, 0.01 equivalence of 100X sodium pyruvate (v/v), and 0.001 equivalence (v/v) of 1000X methionine (final 37.5 mg/L = 250 μM) or 0.01 equivalence (v/v) of 100X AHA (final 250 μM).

Cell lysis and immunoblotting assay

Immunoblotting assay was performed based on previously reported method[5]. Briefly, cells were cultured in the presence of the corresponding stress to 40~50% confluency in 6-well plates, 10 cm or 15 cm dishes. After removing the media, the cells were washed with DPBS three times, then in-house RIPA buffer (50 mM HEPES, 150 mM NaCl, 1% sodium deoxycholate, 1% NP-40, 0.1% SDS, 2.5 mM $MgCl_2$, 10 mM sodium glycerophosphate, 10 mM sodium biphosphate) containing mammalian protease inhibitor cocktail (Sigma), PhosSTOP, and 20 unit/ml Benzonase (Millipore) were added directly onto the cells. Cell lysates were collected by cell scrapers and sonicated on ice three times, followed by centrifugation (13000 rpm, 5 min). The concentration of the supernatant was measured by Bradford assay, and the whole cell lysate was further denatured by the addition of LDS sample buffer supplemented with 100 mM DTT, followed by boiling at 75°C for 5 minutes. 20 or 30 μg of each lysate was loaded onto the 4–20% Tris-Glycine gel (Thermo Fisher Scientific) or 4–12% NuPAGE Bis-Tris gel (Thermo Fisher Scientific), followed by SDS-PAGE with Tris-Glycine SDS running buffer (Thermo Fisher Scientific) or MES SDS running buffer (Thermo Fisher Scientific), respectively. The proteins were electro-transferred to PVDF membranes (0.45 μm, Millipore), and then the total protein was stained by Revert total protein stain kit (LI-COR) or Ponceau staining (Thermo Fisher Scientific). The membrane was then blocked with 5% non-fat milk (r.t., 30 min), incubated with the indicated primary antibodies (4°C, overnight), washed three times with TBST (total 30 min), and further incubated either with fluorescent IRDye 680RD Goat anti-Mouse IgG H+L, IRDye 800RD Goat anti-Mouse IgG H+L, or IRDye 800CW Goat anti-Rabbit IgG H+L secondary antibody (1:15000) for 1 hour. After thorough wash with TBST for 30 min, near infrared signal was detected using OdysseyCLx imager and quantified using ImageStudioLite (LI-COR). For quantitative immunoblotting of endogenously tagged Ribo-Keima reporter cells, at least 70 μg of total lysate was loaded on to SDS-PAGE gel due to low expression level of Keima construct and small amount of processed Keima level. 4–20% Tris-Gly gel was used to resolve the proteins.

Flow-cytometry analysis for one-color Ribo-Halo labeling

Corresponding Ribo-Halo cells were plated onto 24-well plates one day prior to the nutrient stress. The cells were left untreated or treated with 200 nM Torin1 for the indicated hours. 1h before collecting the cells, 100 nM of TMR-ligand was added in addition to the Torin1 for HaloTag labeling. The cells were washed with fresh DMEM with or without Torin1, three times with 10 min duration each. After trypsin treatment, the collected cells were re-suspended in 250 μl FACS buffer (1x DPBS, 1 mM EDTA, 1% FBS, 25 mM HEPES, final pH 7.3–7.5), and analyzed by flow-cytometry (LSR-II Analyser, BD Biosciences). The data was processed by FlowJo software.

Flow-cytometry analysis for two-color Ribo-Halo labeling

Corresponding Ribo-Halo cells were plated onto 24 well plates. 100 nM of TMR-Halo ligand was added and incubated for 1h to label the pre-existing ribosomes, then washed away. The cells were incubated with 2 ml of fresh DMEM for 10 min at dark to remove the remaining free TMR-ligand. This was repeated for three times in total. Then the cells were grown either in rich medium or in Tor1 treatment medium, both containing 50 nM R110 Halo ligand. In parallel, control Ribo-Halo cells were stained only with TMR-ligand or with R110 ligand, the signal of which represented 100% ribosome abundance and used as a normalization factor. The cells were than collected after trypsin treatment, re-suspended in 250 μl FACS buffer (1x DPBS, 1 mM EDTA, 1% FBS, 25 mM HEPES, final pH 7.3–7.5), and analyzed by flow-cytometry (LSR-II Analyser, BD Biosciences). The data was processed by FlowJo software. Briefly, the 488 and 561 nm intensities of individual cells (> 3000 cells) were exported to excel. Each fluorescence signal from the single cells were normalized by the signal intensity from the 100% Red or 100% Green ligand treated cells for the same duration. The old to young ribosome ratio distribution graph was processed by dividing the normalized red signal with the normalized green signal coming from the same single cells and plotted using Prism software.

In-gel fluorescence analysis for two-colored Ribo-Halo labeling

Related to Figs. 2 and 4. Corresponding Ribo-Halo cells were plated onto 12 well plates. 100 nM of TMR-Halo ligand[30] was added and incubated for 1h to label the pre-existing ribosomes, then washed away. The cells were incubated with 2 ml of fresh DMEM for 10 min at dark to remove the remaining free TMR-ligand. This was repeated for three times in total. Then the cells were grown either in rich medium or in Tor1 treatment medium, both containing 50 nM R110 Halo ligand. In parallel, control Ribo-Halo cells were stained only with TMR-ligand or with R110 ligand, the signal of which represented 100% ribosome abundance and used as a normalization factor. The cells were than collected after trypsin treatment, re-suspended in RIPA buffer, and sonicated three times on ice. Following Bradford assay, 15 μg of the lysates were taken from each sample and resolved by SDS-PAGE using a 4–12% NuPAGE Bis-Tris gel (Thermo Fisher Scientific). The in-gel TMR and R110 signals were detected by ChemiDoc™MP (Bio-rad). The gel was then either stained with Coomassie blue staining for loading control, or proteins transferred to PVDF membrane for the subsequent immunoblotting analysis. Ratio change of the TMR and R110 signals were analyzed using Image Lab software (BIO-RAD)

Cell size measurement

Related to Extended Data Figs. 2 and 3. Cells were grown on a 24-well plate with or without Torin1 (200 nM) for 14 hours. Then, the cells were treated with trypsin for 3 min, followed by the addition of 1 ml DMEM. The cells were collected and spun down at 1000 rpm for 3 min, and the DMEM was removed. The cell pellet was resuspended in 500 μl of DMEM with or without Torin1 (200 nM) at room temperature. 75 μl of each sample (~ 2.0×10^5 cells/ml) was injected to Moxi Cassette and the size measured by Moxi GO II. The single cell size measurements were processed by FlowJo and plotted using Prism software.

Confocal microscopy

Related to Figs. 2. Live-cell confocal microscopy was performed based on previously reported method[5]. Briefly, cells were plated onto 35 mm-glass bottom dish (No. 1.5, 14 mm glass diameter, MatTek) pre-treated with poly-L-lysine, then pre-incubated in 100 nM TMR-ligand containing medium for 1 hour. Followed by the washing steps (three times for 10 min each), the cells were incubated with or without Torin1 in the presence of 50 nM R110 Halo ligand for 14 or 24 hours. The media was changed to FluoroBrite™DMEM (Thermo Fisher) before the live cell imaging. The cells were imaged using a Yokogawa CSU-X1 spinning disk confocal with Spectral Applied Research Aurora Borealis modification on a Nikon Ti motorized microscope equipped with a Nikon Plan Apo 60×/1.40 N.A or 100x/1.40 N.A objective lens. Pairs of images for ratiometric analysis of TMR and R110 fluorescence were collected sequentially using 100 mW 488 nm and 100 mW 561 solid state lasers attenuated and controlled with an AOTF (Spectral Applied Research LMM-5), and emission collected with a 525/50 nm or 620/60 nm filter (Chroma Technologies), respectively. Wide-field fluorescence images of Hoeschst were collected using a Lumencor SOLA light source, 395/35nm excitation and 480/40nm emission filters (Chroma Technologies). Both confocal and widefield images were acquired with the same Hamamatsu ORCA-ER cooled CCD camera and MetaMorph software. For the analysis, the equal gamma, brightness, and contrast were applied for each image using FiJi software.

Azidohomoalanine (AHA) incorporation and TMR-in-gel fluorescence analysis for translatome analysis

Related to Fig. 3. WT 293T cells were plated onto 10 cm dish with ~20% confluency 24 h before the experiment. Commercial DMEM media was replaced with in-house prepared DMEM media containing either 250 μM Methionine or 250 μM AHA in addition to the indicated nutrient stress medium. The cells were washed three times with DPBS and lysed by the addition of RIPA buffer and sonication (4 °C, three times). Following Bradford assay, 30 μg of lysate was subjected to immunoblotting for pS6K, pS6, and 4E-BP1 for proper inhibition of mTOR activity quality control. From the remaining lysates, equal protein amount was collected across the samples, reduced by 5 mM TCEP (10 min, room temperature), then alkylated by chloroacetamide (20 mM final concentration, 15 min, room temperature). $CHCl_3$/MeOH precipitation was followed to remove any remaining AHA in the cell lysates. White protein disk was then resuspended in 2% SDS (50 mM HEPES 150 mM NaCl, pH7.2, 2.5 mM TCEP) and sonicated once with a tip sonicator. 10 μl of the resuspended lysate was added with 10 μl of 2X Click-master mix containing 2 mM $CuSO_4$, 2 mM sodium ascorbate, 200 μM TBTA ligand, and 200 μM TMR-alkyne in H_2O. The Click reaction mixture was then incubated at dark for 1 hour (with rocking, room temperature, final sample concentration: 0.825 μg/μl). The mixture was then resolved by SDS-PAGE, and TMR signal detected by ChemiDoc™MP (BIO-RAD) and analyzed by Image Lab software (BIO-RAD).

Azidohomoalanine (AHA) incorporation, Biotin-click, and streptavidin enrichment for translatome analysis

Related to Fig. 3. WT 293T cells were plated onto 10 cm dish with ~20% confluency 24 h before the experiment. Commercial DMEM media was replaced with in-house prepared DMEM media containing either 250 μM Methionine or 250 μM AHA in addition to the indicated nutrient stress. The cells were washed three times with DPBS and lysed by the addition of RIPA buffer and sonication (three times). Following Bradford assay, 30 μg of the lysate was subjected to immunoblotting for pS6K, pS6, and 4E-BP1 for proper inhibition of mTOR activity quality control. We also confirmed that AHA labeling (250 μM) without prior Met withdrawal minimized the effects on mTOR activity using pS6K band intensity[31]. From the remaining lysates, equal protein amount was collected across the samples, then reduced by 5 mM TCEP (10 min, room temperature), and alkylated by chloroacetamide (20 mM final concentration, 15 min, room temperature). $CHCl_3$/MeOH precipitation was followed to remove any remaining AHA in the cell lysates. White protein disk was then resuspended in 2% SDS (50 mM HEPES 150 mM NaCl, pH7.2, 2.5 mM TCEP) and sonicated once with a tip sonicator. At least 1 mg of the lysates resuspended in 2% SDS was taken and reacted with the click reagents (final concentration: 1 mM $CuSO_4$, 1 mM sodium ascorbate, 100 μM TBTA ligand, and 100 μM biotin-alkyne), and the mixture was incubated for 2 hours with rocking at room temperature. $CHCl_3$/MeOH precipitation was followed again to remove excess amount of biotin-alkyne, the lysates resuspended with 200 μl of 2% SDS (TCEP 2.5 mM) and diluted with RIPA to make < 1 mg/ml concentration of the lysate (final SDS concentration is < 0.5%). Meanwhile, 10 μl of high capacity streptavidin agarose beads multiplied by the number of samples (ex. 100 μl for 10 samples, the bead has 10 mg/ml BSA-biotin capture capacity. Therefore, 10 μl bead can roughly capture 100 μg of biotinylated proteins when average MW was assumed to be 66 kDa) were washed with 1 ml RIPA and distributed to 10 × 1.5 ml eppendorf tubes. The lysates were added to the beads, incubated overnight at room temperature. Flow-through was then stored for the quality control, and the beads were washed with RIPA X2, 1 M KCl, 0.1 M Na_2CO_3, 2 M Urea in HEPES buffer × 2, and RIPA × 2. The beads were transferred onto hydrophilic PTFE membrane filter cups, washed with water two times. Completely dried beads were then resuspended in 50 μl of hexafluoroisopropanol (HFIP), incubated for 5 min with shaking and eluted by spinning. 50 μl of HFIP was added to the beads again, the eluates combined, and dried in speedvac for 10 min. (bp of HFIP = 58 °C, volatile). This sample was used for either WB or TMT-MS analysis. Note: as a quality control, we gathered the flow-through and blotted it for streptavidin-IRDye800 for equal capture. Also, the flow-through was precipitated with $CHCl_3$/MeOH method followed by click reaction with TMR-alkyne (an orthogonal alkyne reagent to the biotin-alkyne) to check the efficiency of the click reaction. Based on this method, we concluded that the efficiency of initial click reaction was always over 90% when compared with the negative control that does not contain AHA.

Azidohomoalanine (AHA) incorporation and TMT-MS sample preparation for degradome analysis

Related to Fig. 3. Equal number of the WT 293T cells were plated onto 10 cm dish with ~20% confluency 24 h before the experiment. Commercial DMEM media was replaced with in-house prepared DMEM media containing either 250 μM Methionine or 250 μM AHA and

the cells were incubated for 5 hours for AHA incorporation. The AHA containing medium was removed, and the cells were washed with rich DMEM. The cells were incubated in the rich DMEM supplemented with 10% FBS for 1 hour for the degradation of short-lived proteins with AHA incorporation. Then the control cells were collected immediately by addition of the RIPA buffer (containing 0.5% SDS instead of 0.1%), while the UT and nutrient stress samples were further grown in rich medium or Tor1 200 nM containing medium for 12 hours. To avoid the dilution factor of AHA labeled proteome through cell division, we collected the lysates from the entire dish and processed for quality control immunoblotting without normalizing the total proteome level using Bradford assay. The remaining lysates were reduced by 5 mM TCEP (10 min, room temperature), alkylated by chloroacetamide (20 mM final concentration, 15 min, room temperature), and proteins precipitated by $CHCl_3$/MeOH method. White protein disk was then resuspended in 2% SDS (50 mM HEPES 150 mM NaCl, pH7.2, 2.5 mM TCEP) and sonicated once with a tip sonicator. Small aliquot of the lysates was reacted with TMR alkyne for a quality check, and the rest was clicked with biotin alkyne followed by streptavidin capture. In this case, the beads were washed with more stringent buffers (RIPA X2, 2% SDS X2, 3M Urea X2, 0.1 M Na_2CO_3, RIPA × 2, ddH_2O X3).

Fast nuclear-cytosolic partitioning sample preparation for immunoblotting and TMT-MS analysis

Related to Extended Data Fig. 7. The final protocol used in this study (Method 3 in Extended Data Fig. 7b) was modified from[32]. HEK 293T cells were plated onto 10 cm dishes with ~20% confluency, 24h prior to the experiment. The cells were either left untreated or treated with -AA medium for three hours, then washed three times with DPBS. Then the cells were lysed by adding 800 µl of the lysis buffer (50 mM HEPES pH 7.2, 150 mM NaCl, 0.1% NP-40, 10 mM glycerophosphate, 10 mM sodium biphosphate, protease inhibitor cocktail, 2.5 mM $MgCl_2$) directly on to the dish, the lysates collected by scraping, and pipetted up and down 6 times. Over 90% of the cells showed cell membrane rupture with intact nucleus when observed under the microscope after Trypan blue staining. 50 µl was taken and snap-frozen using liquid nitrogen (whole cell lysate). The rest of the lysate was spun down at 7000 rpm for 30 sec, supernatant taken and snap frozen (cytosolic fraction). The remaining pellet was washed with 1 ml DPBS, spun again at 7000 rpm for 30sec, and supernatant was removed (pellet = nuclear fraction). Nuclear fraction pellet was resuspended in 300 µl RIPA buffer containing benzonase and sonicated for three times. The cytosolic fraction was added with 80 µl of 10X RIPA buffer to equalize the surfactant concentration as in nuclear fraction, and sonicated. Bradford assay was performed using the whole cell lysate, cytosolic fractions and the nuclear fraction. 100 µg of the proteins from both nuclear and cytosolic fractions were taken and processed for MS analysis. 15 µg of each fraction was taken and subjected to immunoblotting as quality control. This method resulted in 3.2~3.6 times more loading of the nuclear fractions compared to the cytosolic fractions when calculated back to the total protein level. This ratio was applied for the final calculation of the nuclear-cytosolic protein abundance in the TMT-MS analysis.

Methods in Extended Data Fig. 7b: Method 1) a. buffer: 1% TritonX, 10 mM β-glycerophosphate, 10 mM sodium pyrophosphate, 40 mM HEPES pH 7.4, 2.5 mM $MgCl_2$,

protease inhibitor cocktail. b. lysis method: the cell lysates were incubated for 15 min at 4 °C with rocking, followed by centrifugation for 5 min at 13K rpm. The pellet was washed with DPBS once and resuspended in RIPA buffer for nuclear fraction. c. total time: ~25 min. Method 2) a. buffer: 0.1% TritonX, 10 mM β-glycerophosphate, 10 mM sodium pyrophosphate, 40 mM HEPES pH 7.4, 2.5 mM $MgCl_2$, protease inhibitor cocktail b. lysis method: the cell lysates incubated for 15 min at 4°C with rocking, followed by centrifugation for 5 min at 13K rpm. The pellet was washed with DPBS once and resuspended in RIPA buffer for nuclear fraction. c. total time: ~25min. Method 3) a. buffer: 0.1% NP40 in DPBS (1 mM KH_2PO_4, 150 mM Sodium Chloride, 5.6 mM Na_2HPO_4, protease inhibitor cocktail, pH 7.3–7.5) b. lysis method: the lysates gathered in the lysis buffer was pipetted for three times and centrifugated at 13K for 10 sec. The pellet was washed with DPBS once and resuspended in RIPA buffer for nuclear fraction. c. total time: ~3 min. Method 4) a. buffer: 0.05% NP40, 10 mM HEPES, 1.5 mM $MgCl_2$, 10 mM KCl, 0.5 mM DTT,~pH 7.3 b. lysis method: the cells were collected in the lysis buffer and sit on ice for 10 min for osmotic cell lysis, followed by centrifugation at 3K rpm for 10 min, 4°C. Supernatant was snap frozen while the pellet was washed with the lysis buffer, and centrifugated for 1 min at 3K rpm. The pellet was resuspended in RIPA buffer for nuclear fraction. c. total time: ~25 min

Proteomics workflow ——An extensive description of proteomics methods and detailed parameters are included in the first sheet of each Supplementary Tables.

Proteomics workflow - Sample preparation.—Samples were reduced and alkylated followed by chloroform-methanol precipitated, reconstituted in 100 mM EPPS (pH 8.5), digested by Lys-C and then by trypsin. Samples were TMT labeled for 60 min at room temperature. After labeling efficiency check, samples were quenched, pooled and desalted for subsequent LC–MS/MS analysis. When indicated, pooled sample was first offline fractionated with bRPLC in a 96-well plate and combined for a total of 24 fractions[33] before desalting and subsequent LC–MS/MS analysis.

Proteomics workflow – data acquisition.—Samples were analyzed on Orbitrap Tribrid Serie mass spectrometers coupled to a Proxeon EASY-nLC pump (ThermoFisher Scientific). Peptides were separated on a 35 cm column packed in-house using a 95 to 110 min gradient. MS^1 data were collected using the Orbitrap (120,000 resolution). MS^2 scans were performed in the ion trap with CID fragmentation (isolation window 0.7 Da; rapid scan; NCE 35%). Each analysis used the Multi-Notch MS^3-based TMT method[34], to reduce ion interference compared to MS^2 quantification, combined in some instance with newly implemented Real Time Search analysis software[35,36], and with the FAIMS Pro Interface (using previously optimized 3 CV parameters for TMT multiplexed samples[37]). MS^3 scans were collected in the Orbitrap using a resolution of 50,000, NCE of 65 (TMT) or 45 (TMTpro). The closeout was set at two peptides per protein per fraction, so that MS^3s were no longer collected for proteins having two peptide-spectrum matches (PSMs) that passed quality filters[36].

Proteomics workflow - data analysis.—Mass spectra were processed using a Comet-based (v2018.01 rev.2) in-house software pipeline[38,39] or Sequest-HT using Proteome Discoverer (v2.3.0.420 - Thermo Fisher Scientific). Database searching included all canonical entries from the Human reference proteome database (UniProt Swiss-Prot - 2019–01) and sequences of common contaminant proteins. Searches were performed using a 20 ppm precursor ion tolerance, and recommended product ion parameters for ion trap ms/ms were used. TMT tags on lysine residues and peptide N termini (+229.163 Da for Amino-TMT or +304.2071 Da for TMTpro) and carbamidomethylation of cysteine residues (+57.021 Da) were set as static modifications, while oxidation of methionine residues (+15.995 Da) was set as a variable modification. For phospho-peptide analysis, +79.9663 Da was set as a variable modification on serine, threonine and tyrosine residues. PSMs were filtered to a 1% false discovery rate (FDR) using linear discriminant analysis as described previously[38]. Using the Picked FDR method[40], proteins were filtered to the target 1% FDR level. Phosphorylation site localization was determined using the AScore algorithm[41]. For reporter ion quantification, a 0.003 Da window around the theoretical m/z of each reporter ion was scanned, and the most intense m/z was used. Reporter ion intensities were adjusted to correct for the isotopic impurities. Peptides were filtered to include only those peptides with a sufficient summed signal-to-noise ratio across all TMT channels. An isolation purity of at least 0.7 (70%) in the MS1 isolation window was used for samples analyzed without online real-time searching. For each protein, the filtered peptide TMT or TMTpro signal-to-noise values were summed to create protein quantification values[38].

Protein quantification values were exported for further analysis in Microsoft Excel and Perseus[42] and statistical test and parameters used are indicated in the corresponding Supplementary Tables datasets. Briefly, two-way Welch's t-test analysis was performed to compare two datasets, using s0 parameter (in essence a minimal fold change cut-off) and correction for multiple comparison was achieved by the permutation-based FDR method, both functions that are built-in in Perseus software. For whole cell proteome analysis, each reporter ion channel was summed across all quantified proteins and normalized assuming equal protein loading of all samples. For AHA-derived translatome, as well as Nuclear/Cytosolic fractionation, no normalization based on loading was performed. For AHA-derived degradome normalization, we used a previously reported strategy[43], which is based on the assumption that there are stable proteins within the pool of proteins measured, whose amounts decay very little during the time course of the experiment.

Supplementary Tables list all quantified proteins as well as associated TMT reporter intensity and ratio change to control channels used for quantitative analysis.

Annotations for bona fide organellar protein markers were assembled using the proteins which had scored with confidence "very high" or "high" from the HeLa dataset previously published[44]. Annotations for Ribosome and Autophagy Components were manually curated and assembled based on literature. Nuclear annotations are based on this paper's dataset (Supplementary Table 4).

Statistics

All statistical data were calculated using GraphPad Prism 7 or Perseus. Comparisons of data were performed by two-way ANOVA with Tukey's multiple comparisons test; p-values <0.01 were considered significant.

Reproducibility

All experiments were repeated at least three times unless otherwise indicated.

Data reporting

No statistical methods were used to predetermine sample size. The experiments were not randomized, and the investigators were not blinded to allocation during experiments and outcome assessment.

Reporting summary

Further information on research design is available in the Nature Research Reporting Summary linked to this paper.

Extended Data

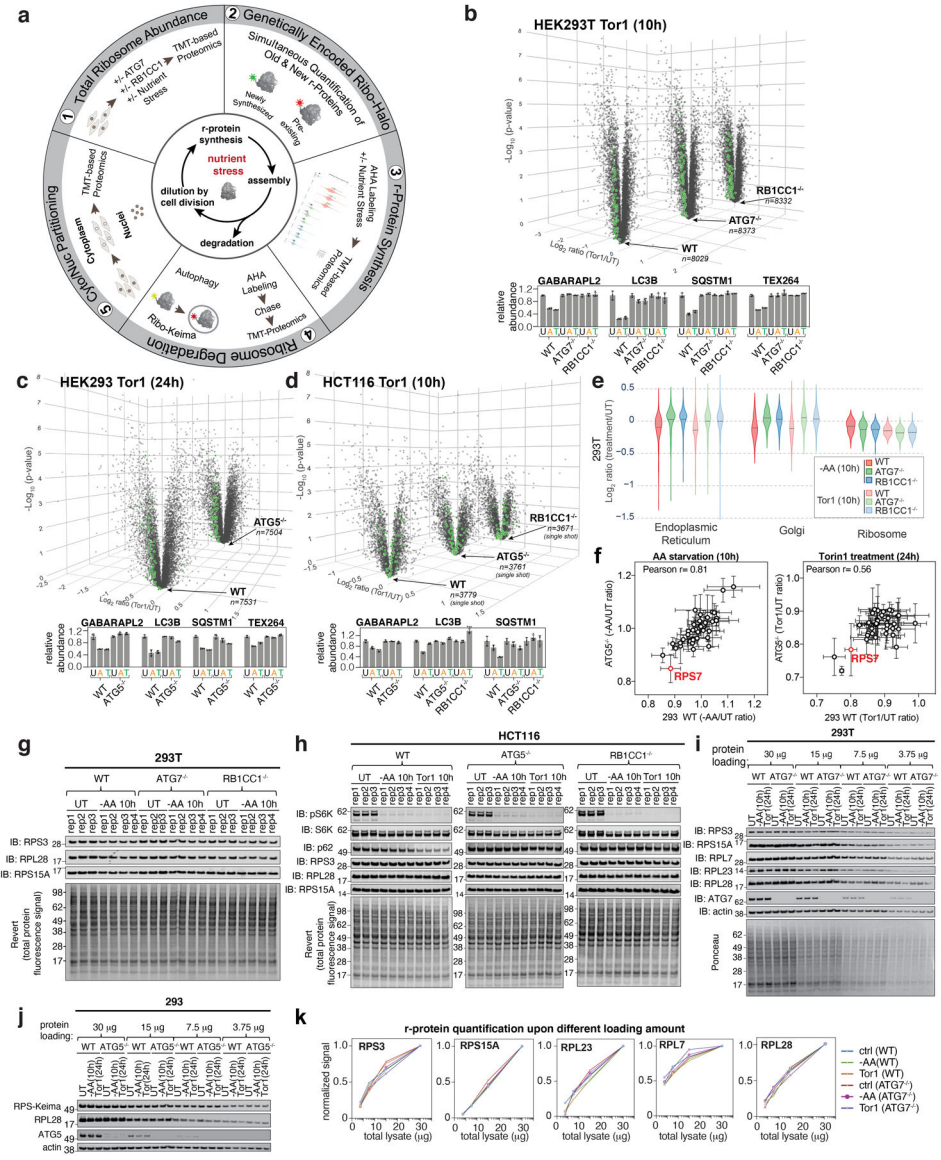

Extended Data Fig. 1 |. Reduction of r-proteins upon nutrient stress is not discernable by immunoblotting methods regardless of autophagy.

a, Schematic of the ribosome analysis pipeline. **b-d**, (top panels) Volcano plots ($-\text{Log}_{10}$ p-value versus Log_2 ratio Tor1/UT) for 293T cells (n=8029 proteins), ATG7$^{-/-}$ (n=8373 proteins) or RB1CC1$^{-/-}$ (n=8332 proteins) (panel b), 293 cells (n=7531 proteins), ATG5$^{-/-}$ (n=7504 proteins) (panel c), or HCT116 cells (n=3779 proteins), ATG5$^{-/-}$ (n=3761 proteins) or RB1CC1$^{-/-}$ (n=3671 proteins) (panel d). n=3 (WT); 4 (Tor1) biologically independent samples. For two-sided Welch's t-test (adjusted for multiple comparison) parameters, individual p-values and q-values, see Supplementary Table 1. Green dots represent ribosomal proteins. Data for 293T cells is from[12]. Histograms below the individual volcano plots show the mean ± SD of relative abundance of autophagy adaptors with or without nutrient deprivation. n=3 (WT) or n=4 (-AA and Tor1) biologically independent samples. U, untreated; A, -AAs; T, Tor1. Data for 293T cells was from[12]. **e**, The relative abundance changes[12] for proteins located in either the endoplasmic reticulum, Golgi, or the ribosome in

293T cells treated as in panel b are plotted as a violin plot (n=340, 349, 343, 340, 349, 343, 87, 89, 86, 87, 89, 86, 72, 75, 70, 72, 75, and 70 proteins, from left to right). Ribosomal protein abundance change is not affected by autophagy unlike other vesicular organelles. The violin curves represent the distribution and density of the indicated dataset (Center-line: median; Limits: minima and maxima). **f**, Plots of relative abundance of individual r-protein in 293 cells upon either 10h of AA withdrawal (left panel) or Tor1 treatment (right panel). 39 r-proteins with less than ±10% error range for every condition are plotted. Mean ±SD for n=3 (WT) or n=4 (-AA and Tor1) biologically independent samples. **g**, 293T cells with or without ATG7 or RB1CC1 were either left untreated, subjected to AA withdrawal (10h) or treated with Tor1 (10h) and whole cell extracts immunoblotted for the indicated proteins. **h**, HCT116 cells with or without ATG5 or RB1CC1 were treated as indicated, and whole cell extracts immunoblotted for the indicated proteins. **i-k**, Extracts from the indicated cells (30, 15, 7.5 or 3.75 μg) were immunoblotted with the indicated antibodies (panels i,j). The signal intensity for the indicated r-proteins as a function of quantity loaded was measured using Odyssey (panel k), showing no indication of signal saturation and no detectable difference between cells with or without active autophagy. Related to Fig. 1. The experiments shown in panels g-j were repeated more than three times independently and showed similar results. For gel source data, see Supplementary Fig. 1.

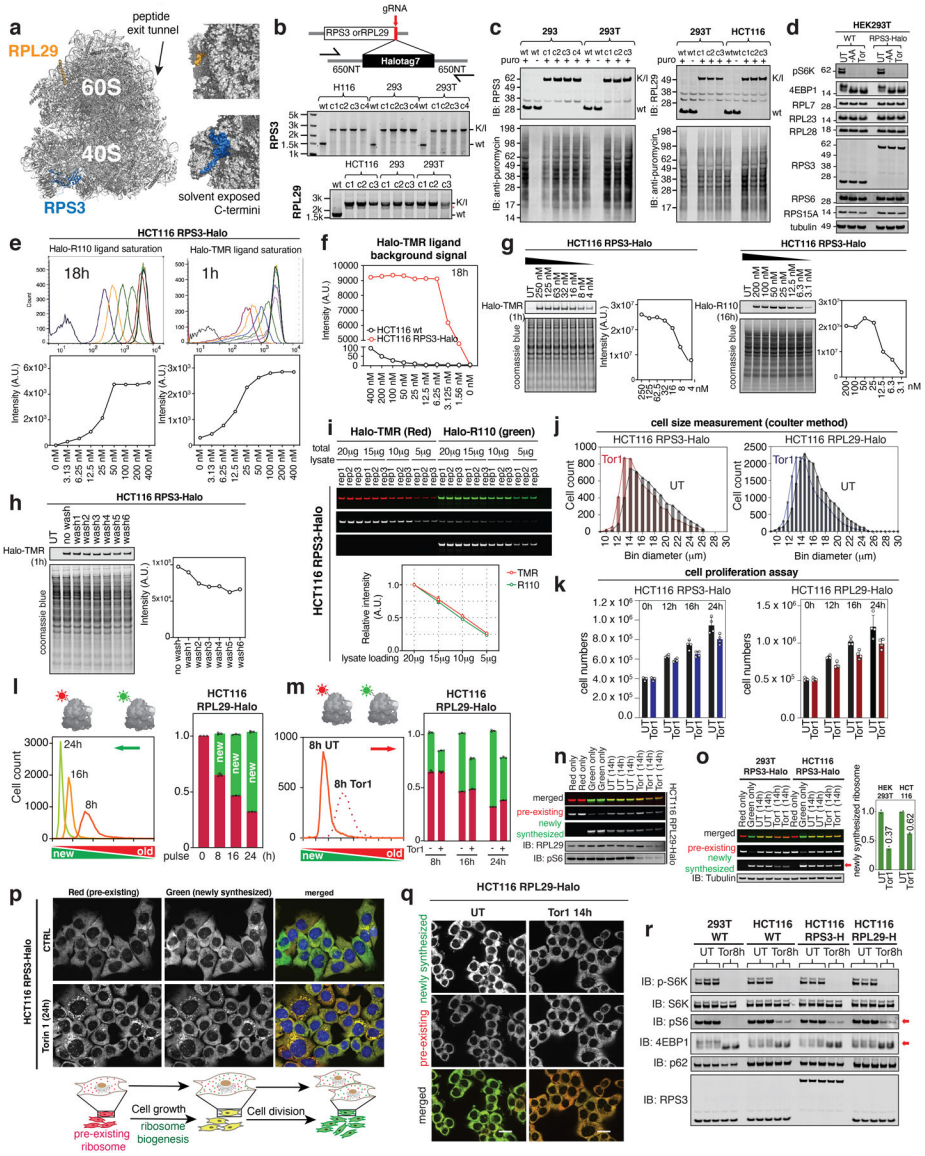

Extended Data Fig. 2 |. Generation of Ribo-Halo reporters and extensive titration assays for quantification.

a, The Halotag7 protein (referred to here as “Halo”) was endogenously tagged at the C terminus of RPL29 or RPS3 as the indicated r-proteins contain solvent exposed C-termini and are located far from the peptide exit tunnel based on the structure of an 80S complex. (PDB: 5AJ0). **b,c**, Gene editing of HCT116, 293, and 293T cells using CRISPR-Cas9 to fuse Halo with the C-termini of RPS3 and RPL29. Homozygous incorporation of Halo was confirmed by genotyping (panel b). Extracts from the indicated cells were subjected to immunoblotting with RPS3 (panel c, left) or RPL29 (panel c, right). Protein translation efficiency of wild-type and Halo knock-in cells were compared using puromycin incorporation assay (panel c, bottom). **d**, Immunoblotting of WT or RPS3-Halo 293T cell lysates after nutrient stress, confirming no detectable difference between the two cell lines in response to mTOR inhibition. The full immunoblot is shown in Extended Data Fig. 9i. **e-g**, Halo-ligand titration assays with the indicated incubation time were performed using flow-

cytometry analysis (panels e and f) or in-gel fluorescence analysis (panel g) for the labeling saturation. In panel f, background signal from free Halo-ligand was measured using WT HCT116 cells in comparison to RPS3-Halo, confirming that the free ligand does not contribute to the observed fluorescence signal. **h**, HCT116 RPS3-Halo cells were incubated with 250 nM Halo-TMR ligand for 1h, washed for indicated numbers by incubating cells in ligand free medium for 20 minute each time, followed by 17h prolonged incubation in ligand free medium. **i**, Extracts from the RPS3-Halo HCT116 cells (20, 15, 10 or 5 μg) treated with the indicated Halo ligands were subjected to in-gel fluorescence analysis. The fluorescence signal intensity of each lane was directly proportional to the loading amount. We noted that R110 fluorophore was excited by epi-green excitation (520–545 nm) and detected in 577–613 nm. We subtracted this bleed-through signal for TMR quantification. **j**, Measurement of the effect of Tor1 on cell size with HCT116 RPS3-Halo (left) and RPL29-Halo (right) using Coulter Principle-based cell measurements. **k**, Cell proliferation assay. HCT116 RPS3-Halo and RPL29-Halo cells were grown in rich medium or Tor1 (200 nM) containing medium for 12h, 16h, and 24h. The data estimates ~16h cell division rate for untreated cells, and ~24h cell division rate for Tor1 treated cells. Mean ±SD for n=4 biologically independent experiments. **l**, Ratio of pre-existing to newly synthesized RPL29-Halo per cell plotted against cell populations as a frequency histogram (left panel). Average from the triplicate experiments plotted as a bar graph (right panel). Pre-existing Ribo-Halo proteins in HCT116 RPL29-Halo cells were labeled with TMR-ligand (100 nM, 1h), followed by the thorough washing and addition of 50 nM Green-ligand (also called R110-ligand). The newly synthesized RPL29-Halo was chased for 8, 16, and 24 hours prior to flow-cytometry analysis. Error bars represent SD. See METHODS for details. **m**, Pre-existing RPL29-Halo proteins were labeled with TMR-ligand (100 nM, 1h) in HCT116 cells, and the newly synthesized RPL29-Halo in the presence or absence of Tor1 (200 nM) were labeled with Green-ligand. The ratio of R110 to TMR signals plotted against cell populations (left panel), and the mean values from the triplicate experiments of 8h, 16h, and 24h pulse chase plotted as a bar graph (right panel) are shown. Error bars represent SD. **n**, In-gel fluorescence images of the cell extracts treated as in panel m. The same gels were then transferred to PVDF membranes for immunoblotting measurement of total RPL29 level. n=3 biologically independent samples are shown. **o**, In-gel fluorescence images of the cell extracts from 293T RPS3-Halo or HCT116 RPS3-Halo cells using the labeling strategy in panel m. Relative synthesis of RPS3-Halo with or without Tor1 is plotted on the right. Mean for n=2 experiments. **p**, Live-cell imaging of HCT116 RPS3-Halo cells labeled with TMR (for pre-existing r-proteins) and Green (for newly synthesized r-proteins) ligands with or without Tor1 (200 nM, 24h). Scale bar = 20 μm. **q**, Live-cell imaging of HCT116 RPL29-Halo cells labeled with TMR (for pre-existing r-proteins) and Green (for newly synthesized r-proteins) ligands with or without Tor1 (200 nM, 14h). Scale bar = 20 μm. **r**, The indicated cells were left untreated or incubated with Tor1 for 8h prior to immunoblotting with the indicated antibodies. Related to Fig. 2. The experiments in panels d, j, and p-r were repeated three times independently and showed the similar results, and panels b-c and e-i were performed once. For gel source data, see Supplementary Fig. 1.

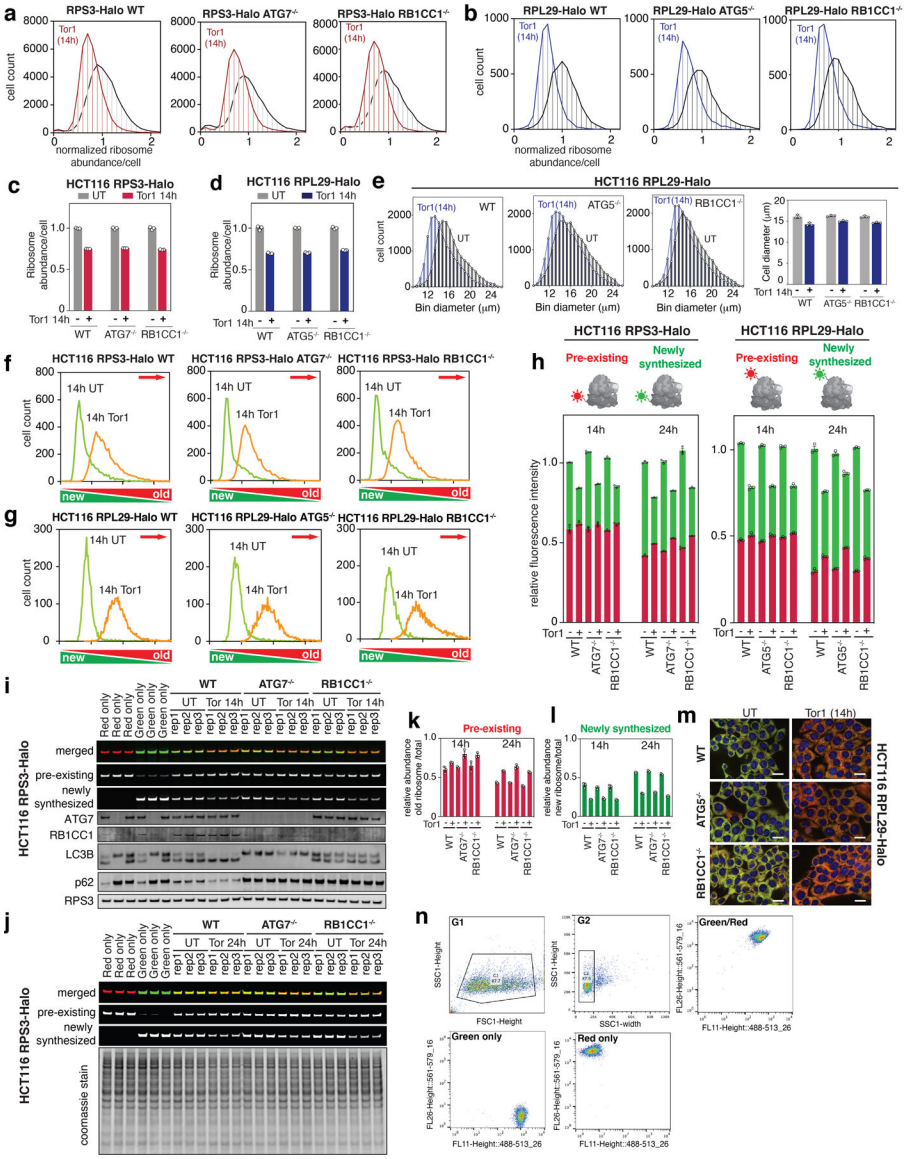

Extended Data Fig. 3 |. Minimal contribution of ribophagy to control of r-protein synthesis and dilution by cell division in response to nutrient stress.

a,b, Histogram of normalized TMR signal in RPS3-Halo (panel a) and RPL29-Halo (panel b) HCT116 cells with or without ATG8 conjugation (ATG7 for RPS3-Halo and ATG5 for RPL29-Halo) or RB1CC1 incubated with or without 200 nM Tor1 for 14h, followed by 1h TMR ligand treatment and flow-cytometry analysis. $>3\times10^5$ and $>4\times10^3$ cells were analyzed, respectively. **c,d**, Mean of the triplicate data from cells treated as in panel a and b are plotted, respectively. Error bars represent SD. **e**, Effect of Tor1 treatment on cell size in HCT116 RPL29-Halo WT, ATG5$^{-/-}$ and RB1CC1$^{-/-}$ cells, as measured using Coulter Principle-based cell measurements. Mean ± SD of the triplicate data is plotted. **f,g**, Ratio of pre-existing (red) to newly synthesized (green) r-proteins per cell plotted against cell populations as a frequency histogram for RPS3-Halo (panel f) or RPL29-Halo (panel g) HCT116 cells with or without ATG5/7 or RB1CC1 based on the labeling scheme in Fig. 2f. **h**, Quantification of relative amounts of pre-existing and newly synthesized r-proteins from

data in panels f and g. Mean ± SD, n=3 biologically independent experiments. **i,j**, HCT116 RPS3-Halo cells with or without ATG7 or RB1CC1 were left untreated or treated with Tor1 for 14h (panel i) and 24h (panel j) using the Halo tagging scheme in Fig. 2f. Extracts were subjected to SDS-PAGE and in-gel fluorescence analysis, followed by immunoblotting with the indicated antibodies. **k,l**, Quantification of relative amounts of pre-existing and newly synthesized r-proteins from data in panels i and j. Mean ± SD, n=3 biologically independent experiments. **m**, Live-cell imaging of HCT116 RPL29-Halo cells with indicated genotypes labeled with TMR (for pre-existing r-proteins) and Green (for newly synthesized r-proteins) ligands with or without Tor1 (200 nM, 14h). Scale bar = 20 μm. **n,** An example of gating strategy used for flow-cytometry analysis. Green and Red only control experiments are shown at the bottom. Experiments in panels m and n were repeated more than three times independently with similar results. For gel source data, see Supplementary Fig. 1.

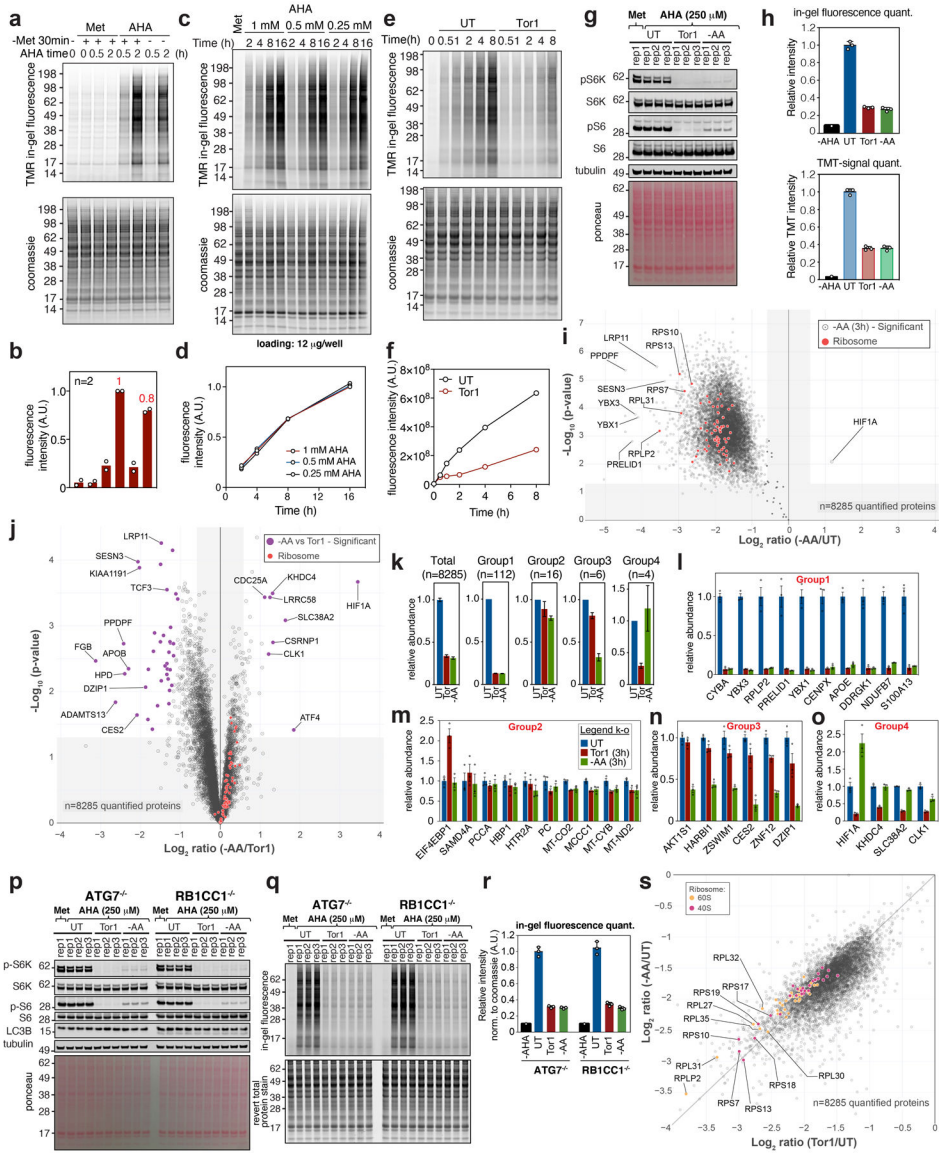

Extended Data Fig. 4 |. Global decoding of protein translation during nutrient stress via independent AHA-TMT methods.

a,b, Total AHA incorporation levels with or without prior Methionine starvation (30 min) were compared using 293T cells grown in Met or AHA (250 μM) for the indicated duration, followed by click with TMR alkyne and in-gel fluorescence analysis (panel a). The quantification of duplicate experiments is shown in panel b. **c,d**, 293T cells were grown in media with Met (250 μM) or the indicated concentration of AHA for the indicated time periods. Extracts were clicked with TMR and subjected to SDS-PAGE prior to Coomassie staining or in-gel TMR fluorescence analysis (panel c). TMR intensity was quantified in panel d. **e,f**, 293T cells grown in AHA (250 μM) with or without To1 for the indicated time periods and extracts clicked with TMR prior to processing as in panel c. The effect of Tor1 on TMR fluorescence is quantified in panel f. **g**, 293T cells were incubated with or without AA withdrawal or Tor1 containing media in the presence of Met or AHA (250 μM each), as in Fig. 3c. Cell extracts were subjected to SDS-PAGE followed by immunoblotting. Three

biologically independent samples are shown in the same blot. **h**, TMR signals in Fig. 3c. were quantified as described in METHODS and plotted in top panel, and the relative TMT signal of the total biotinylated proteome in Fig. 3d. is plotted in bottom panel. Centre data are mean ±SD. n=1, 3, 3 and 3 biologically independent samples, from left to right for top and bottom panels. **i**, Translatome analysis. 293T cells were carried through the workflow in Fig. 3b with AA withdrawal and extracts clicked with biotin prior to enrichment on streptavidin and TMT-based proteomics. Plot of $-\text{Log}_{10}$ p-value versus Log_2 ratio -AA/untreated is shown for n=8285 proteins. For two-sided Welch's t-test (adjusted for multiple comparison) parameters, individual p-values and q-values, see Supplementary Table 2. n=3 (UT; -AA) biologically independent samples. **j**, Translatome plot of $-\text{Log}_{10}$ p-value versus Log_2 ratio -AA/Tor1 is shown (n=8285 proteins). r-proteins skewed to the right side of the volcano plot indicates that Tor1 suppresses the translation of r-proteins more strongly than -AA, unlike the majority of the proteome. For two-sided Welch's t-test (adjusted for multiple comparison) parameters, individual p-values and q-values, see Supplementary Table 2. n=3 (-AA; Tor1) biologically independent samples. **k-o**, The relative abundance of all quantified biotinylated proteins are shown in panel k. Proteins in individual groups are shown in panels l-o. l: representative proteins showing over 2-fold more reduction in translation than the average translation in both Tor1 and -AA conditions, m: proteins with over 2-fold less reduction in translation than the average translation in both Tor1 and -AA conditions, n: proteins showing 2-fold less reduction only in Tor1 condition, with *p*-value (Supplementary Table 2) between Tor1 and -AA was less than 0.05. o: proteins showing 2-fold less reduction only in -AA condition, with *p*-value (Supplementary Table 2) between Tor1 and -AA was less than 0.05. n = 3 biologically independent samples per conditions (UT; -AA; Tor1). Centre data are mean ±S.E.M. **p-r**, 293T cells lacking either ATG7 or RB1CC1 were subjected to AA withdrawal or Tor1 treatment for 3h in the presence of 250 μM Met or AHA. Cell extracts were subjected to SDS-PAGE followed by immunoblotting with the indicated antibodies (panel p) or clicked with TMR and in-gel fluorescence analysis (panel q). TMR signals were quantified as described in METHODS (panel r). Centre data are mean ±SD. n=1, 3, 3 and 3 biologically independent samples, from left to right. **s**, Correlation plot (Log_2 ratio of treated/untreated) for the translatome upon either Tor1 treatment or AA withdrawal. Related to Fig. 3. Experiments in c-f were performed once and p was performed three times independently with similar results. For gel source data, see Supplementary Fig. 1.

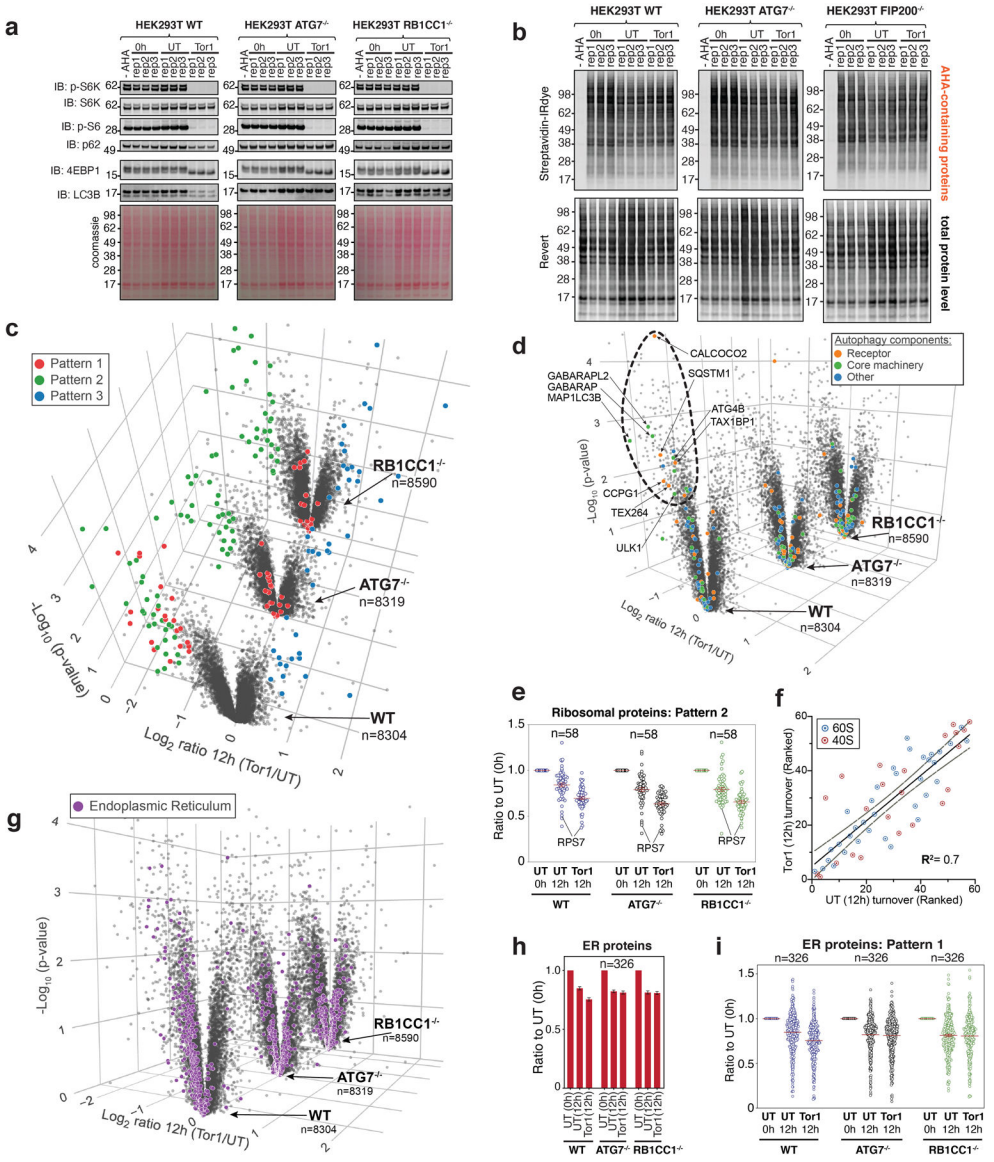

Extended Data Fig. 5 |. Global decoding of protein degradation during nutrient stress via independent AHA-TMT methods.

a, Extracts from cells as described in Fig. 3g were subjected to immunoblotting with the indicated antibodies to demonstrate suppression of the mTOR activity by Tor1. **b**, Biotinylated extracts as described in Fig. 3g were subjected to immunoblotting with a fluorescent streptavidin conjugant, showing the pre-existing proteome (Streptavidin-IRdye) versus the total proteome (Revert total protein stain) in the lysates. n=3 biologically independent samples are shown in a and b. **c,** Volcano plots ($-\text{Log}_{10}$ p-value versus Log_2 Tor1/UT 12h) for 293T WT (n=8304 proteins), ATG7$^{-/-}$ (n=8319 proteins), and RB1CC1$^{-/-}$ (n=8590 proteins) cells as in Fig. 3i, but with pattern 1 proteins in Fig. 3h colored as red dots, pattern 2 proteins colored as green dots, and pattern 3 proteins colored as blue dots. For two-sided Welch's t-test (adjusted for multiple comparison) parameters, individual p-values and q-values, see Supplementary Table 3. n=3 (UT; Tor1) biologically independent samples. **d**, Volcano plots as in panel c, but with autophagy related proteins colored as indicated.

Autophagy adaptors dramatically degraded upon Tor1 treatment only in WT cells are shown in the circle. **e**, Plots of individual ratio for AHA-labeled ribosomal proteins employing the protocol in Fig. 3g in WT, ATG7$^{-/-}$, or RB1CC1$^{-/-}$ 293T cells. r-proteins with STDEV < 0.3 for every condition are selected (n=58 r-proteins). Centre data are mean ±SD from 3 biologically independent samples for each condition. **f**, Relative turnover rates for individual r-proteins from panel e, with or without mTOR inhibition have a correlation of R^2~0.7 (n=58 r-proteins). Grey dotted lines are 95% confidence intervals of the best-fit line (solid black line) result from a simple linear regression analysis. **g**, Volcano plots as in panel d, but with ER resident proteins colored in purple. **h,i**, Individual ratio for n=326 AHA-labeled ER membrane resident proteins employing the protocol in Fig. 3g in WT, ATG7$^{-/-}$, or RB1CC1$^{-/-}$ 293T cells (panel h) and plots for all individual ER resident proteins data points used in h (panel i). Centre data are mean ±SEM. **Related to Fig. 3.** For gel source data, see Supplementary Fig. 1.

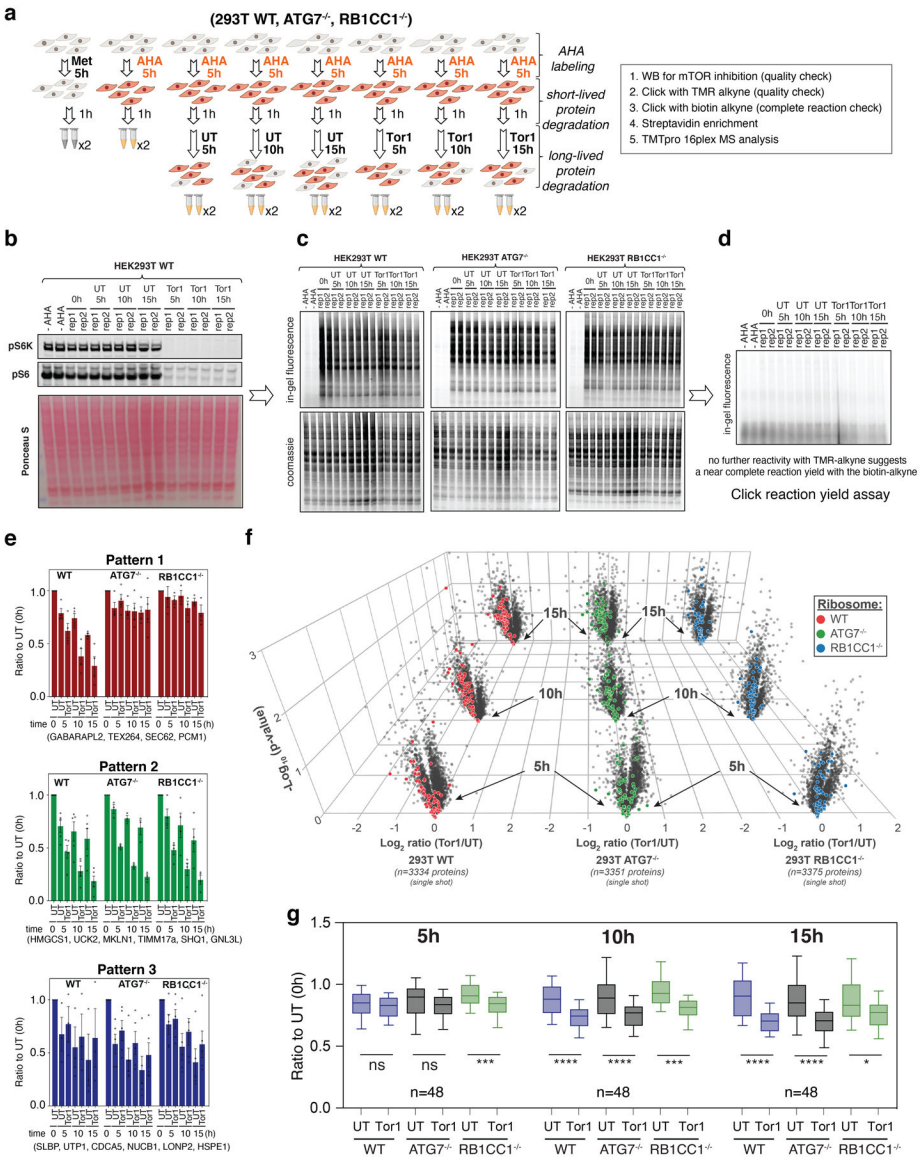

Extended Data Fig. 6 |. Protein degradation time-course during nutrient stress via AHA-TMT methods.

a, Schematic of AHA-based degradomics time-course to examine r-protein turnover during nutrient stress with or without functional autophagy. **b**, Lysates from 293T cells treated as in panel a, were subjected to SDS-PAGE followed by immunoblotting to confirm proper mTOR inhibition. **c**, Cell extracts were reacted with TMR alkyne for click reaction followed by in-gel fluorescence analysis. **d**, Click reaction yield across the replicates was confirmed indirectly. Briefly, cell extracts treated as in panel a, were clicked with biotin alkyne followed by streptavidin capture. The proteins in the flow-though was precipitated, re-suspended in 2% SDS, then clicked with TMR-alkyne. **e**, Patterns of protein turnover, as described in the main Fig. 3h, in the time-course experiment. mean ±SEM. Proteins analyzed (n=4 top; n=6 middle and bottom) are shown below. **f**, Volcano plots for the indicated time ($-\text{Log}_{10}$ p-value versus Log_2 Tor1/UT) in 293T WT (n=3334 proteins), ATG7$^{-/-}$ (n=3351 proteins), and RB1CC1$^{-/-}$ (n=3375 proteins) cells. r-proteins, red, green

or blue. For two-sided Welch's t-test (adjusted for multiple comparison) parameters, individual p-values and q-values, see Supplementary Table 3. **g**, A boxplot of the individual ratio for AHA-labeled ribosomal proteins employing the protocol in panel a (center line, median; box limits correspond to the first and third quartiles; whiskers, 10–90 percentiles range). n=48 r-proteins that were quantified across WT, ATG7$^{-/-}$, and RB1CC1$^{-/-}$ 293T cells. two-sided t-test, p = 0.1514, 0.2818, 0.0005, 0.000016, 0.000051, 0.0005, 0.000001, 0.000020, 0.0105 from left to right) *ns=non-significant, *P<0.1, ***P<0.001, ****P<0.0001.* Experiments in b-d were replicated twice independently and showed similar results. For gel source data, see Supplementary Fig. 1.

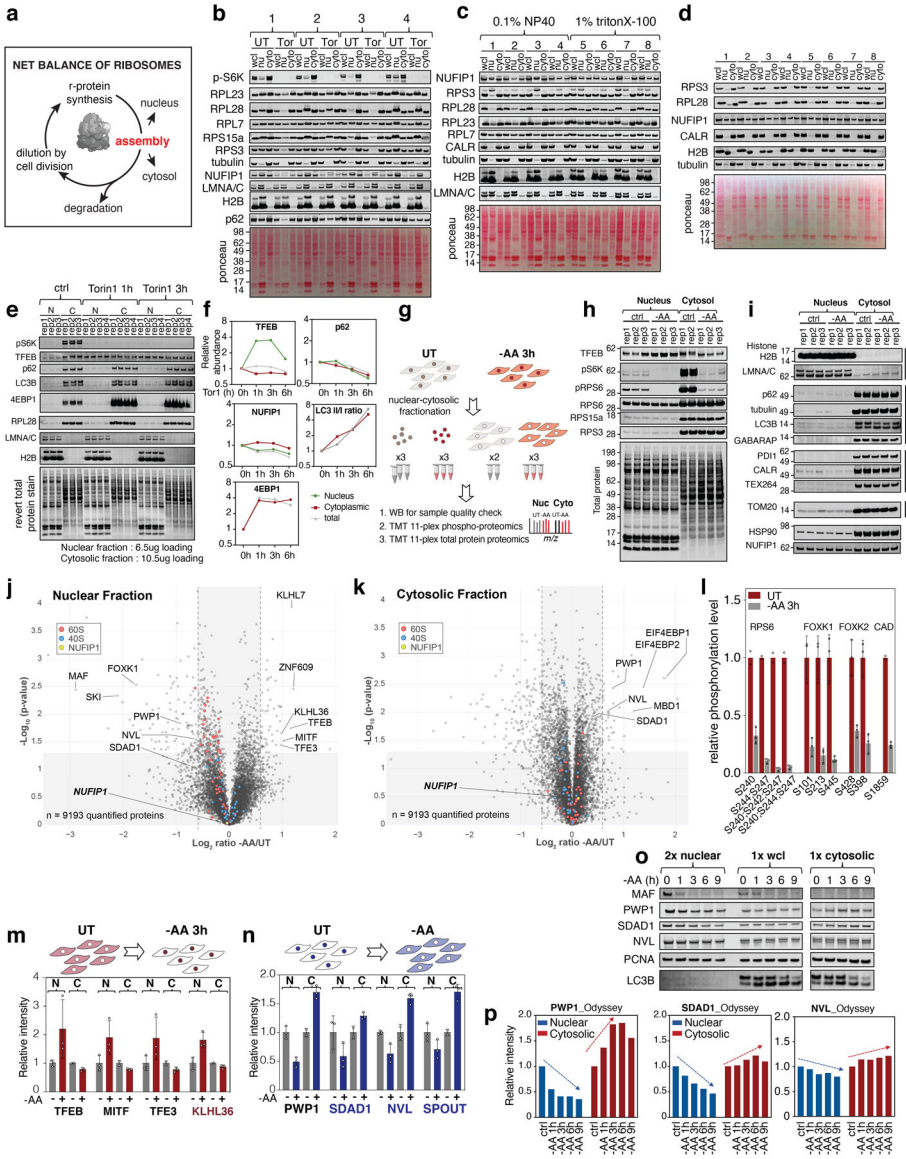

Extended Data Fig. 7 |. Optimization of nuclear-cytosolic partitioning during nutrient stress.

a, Contribution of cytoplasmic and nuclear partitioning to net ribosome balance upon nutrient stress. **b,c**, Optimization of the nuclear and cytosolic fraction partitioning method using 293T cells. Side by side comparison of four previously published methods was performed. Surfactant used in method1: 1% Triton, method 2: 0.1% Triton, method 3: 0.1% NP40, method 4: 0.05% NP40. For more details on method 1–4, see METHOD. Method 2 and 3 were further compared in panel c. 1: ctrl, 2: Leptomycin B (20 nM, 16h), 3: $MgCl_2$ added in lysis buffer, 4: 2+3, 5: ctrl, 6: Leptomycin B (20 nM, 16h), 7: $MgCl_2$ added in lysis buffer, 8: additional pipetting. **d**, Effect of the centrifugal velocity and duration on nuclear-cytosol partitioning is shown. 1: 13K rpm, 10sec, 2: 10K rpm, 10sec, 3: 7K rpm, 10sec, 4: 7K rpm, 30sec, 5: 5K rpm, 60sec, 6: 5K rpm, 180sec, 7: 3K rpm, 60sec, 8: 3K rpm, 180sec. **e,f**, Lysates collected after Tor1 treatment for 0h, 1h or 3h subjected to the optimized nuclear-cytosol partitioning, followed by immunoblotting against the indicated antibodies

(panel e). Quantification measured by Odyssey shown in panel f. **g**, Scheme depicting strategy for quantitative analysis of changes in nuclear and cytosolic protein abundance in 293T cells in response to short period (3h) of AA withdrawal. **h,i**, Biochemical characterization of nuclear and cytosolic 293T cell fractions in response to AA withdrawal. Extracts (15 μg of cytosol and nuclei) were separated by SDS-PAGE and immunoblots probed with the indicated antibodies (see METHODS). **j,k**, Volcano plots ($-\text{Log}_{10}$ p-value versus Log_2 -AA/UT) for nuclear (j) or cytosolic (k) proteins (n=9193 proteins) quantified by TMT-based proteomics. For two-sided Welch's t-test (adjusted for multiple comparison) parameters, individual p-values and q-values, see Supplementary Table 4. Nuclear fraction (j) n=3 (UT; -AA), cytosolic fraction (k) n=2 (UT); n=3 (-AA) biologically independent samples. **l**, Relative RPS6, FOXK1, FOXK2, and CAD phospho-peptides abundance quantified by TMT-based proteomics confirming strong inhibition of mTOR by Tor1. Centre data are mean ±SD. n=2 for UT RPS6 and CAD, and 3 for the rest. **m,n**, Relative abundance of proteins that translocate either from cytosol to nucleus (panel m) or from nucleus to cytosol (panel n) after 3h AA withdrawal, including proteins linked with nutrient dependent transcription (TFEB, MITF, TFE3 – accumulating in the nucleus), and proteins involved in ribosome assembly (PWP1, SDAD1, NVL – exported from the nucleus to the cytosol). Centre data are mean ±SD. n=3, 2, 3 and 3 biologically independent samples, from left to right for each indicated proteins. **o,p**, 293T cells were treated with -AA medium for the indicated time period, partitioned into nuclear and cytosolic fractions, followed by immunoblotting against the indicated antibodies (panel o). Odyssey quantification shown in panel p. Experiments shown in b-d were performed once, e,h,i were performed more than three times independently with similar results, and o was performed twice with similar results. For gel source data, see Supplementary Fig. 1.

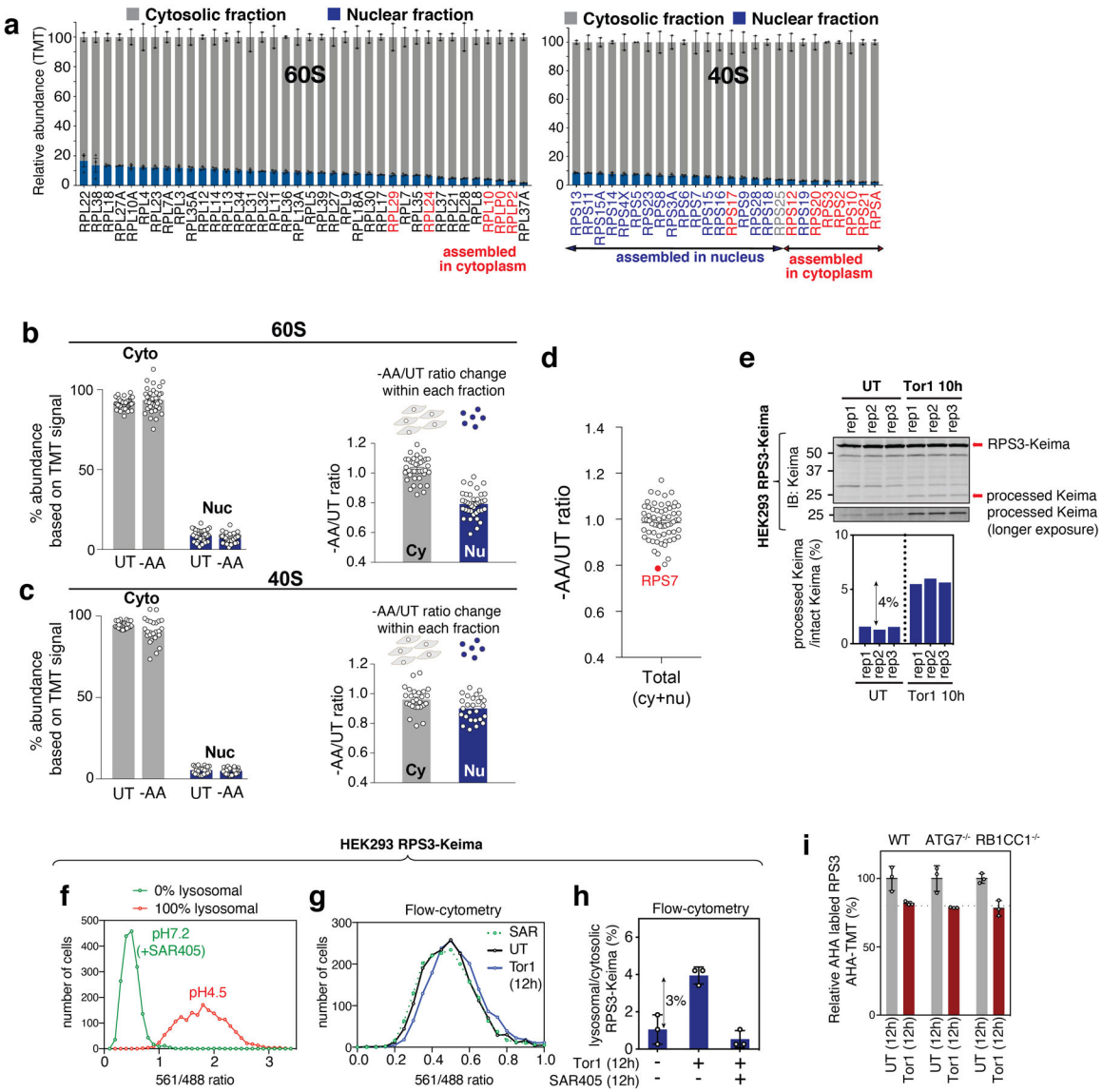

Extended Data Fig. 8 |. Contribution of nuclear-cytosolic partitioning to r-protein abundance during nutrient stress and ribophagy flux measurement using Ribo-Keima system.

a, Relative abundance of individual r-proteins from the 60S subunit (left) or 40S subunit (right) with the cytosol fraction in grey and the nuclear fraction in blue. (less than ±10% error range for every replicate) Individual r-proteins that are thought to assemble onto the ribosome either late in the assembly process or specifically in the cytosol are indicated in red font. mean ±SD. n=2 for cytosolic fraction and 3 for nuclear fraction as shown in Extended Data Fig. 7g. **b,c**, Abundance of nuclear and cytosolic r-proteins after AA withdrawal (3h). 60S subunits are on top (n=38), and 40S subunits are at the bottom (n=26). Right panels indicate the relative r-protein abundance change normalized by UT of cytosolic or nuclear fraction. mean ±SEM. **d**, -AA/UT ratio of individual r-proteins from both nuclear and cytosolic fractions collected after 3h AA starvation indicates heterogenous distribution with RPS7 most strongly down regulated. n=64, mean ±SEM. **e**, Lysates from HEK293 RPS3-Keima cells after the indicated nutrient stress were immunoblotted against anti-Keima

antibody (top). Abundance ratio of the processed Keima to the intact Keima measured by Odyssey is plotted (bottom). **f**, Flow-cytometry analysis of HEK293 RPS3-Keima cells to obtain normalization factors. To achieve a condition in which cells have 0% of the ribosomes in the lysosome, RPS3-Keima cells were treated with SAR405 for 10h and collected in pH7.2 FACS buffer. To achieve a theoretical condition in which 100% ribosomes are present in the lysosome, the cells were incubated in pH4.5 FACS buffer containing 0.1% Triton-X. We used the 561/488 ratio from these two measurements to calculate the % lysosomal ribosomes in panels g and h. n=1742 cells for each. **g,h**, HEK293 RPS3-Keima cells were left untreated or treated with Tor1 (200 nM) in the presence or absence of SAR405 (1 μM) for 12 hours. 561 nm ex to 488 nm ex Keima signal was measured by flow-cytometry and plotted as either a frequency histogram (panel g, n=1742 cells for each) or a bar graph (panel h, n=3 biologically independent samples, mean ±SD). **i**, TMT-based quantification of endogenous RPS3 abundance in 293T WT, ATG7$^{-/-}$, and RB1CC1$^{-/-}$ cells treated and processed as in Fig. 3g. n=3 biologically independent samples. mean ±SD. Experiments in e,g,h were repeated three times independently with similar results, and f was repeated once. For gel source data, see Supplementary Fig. 1.

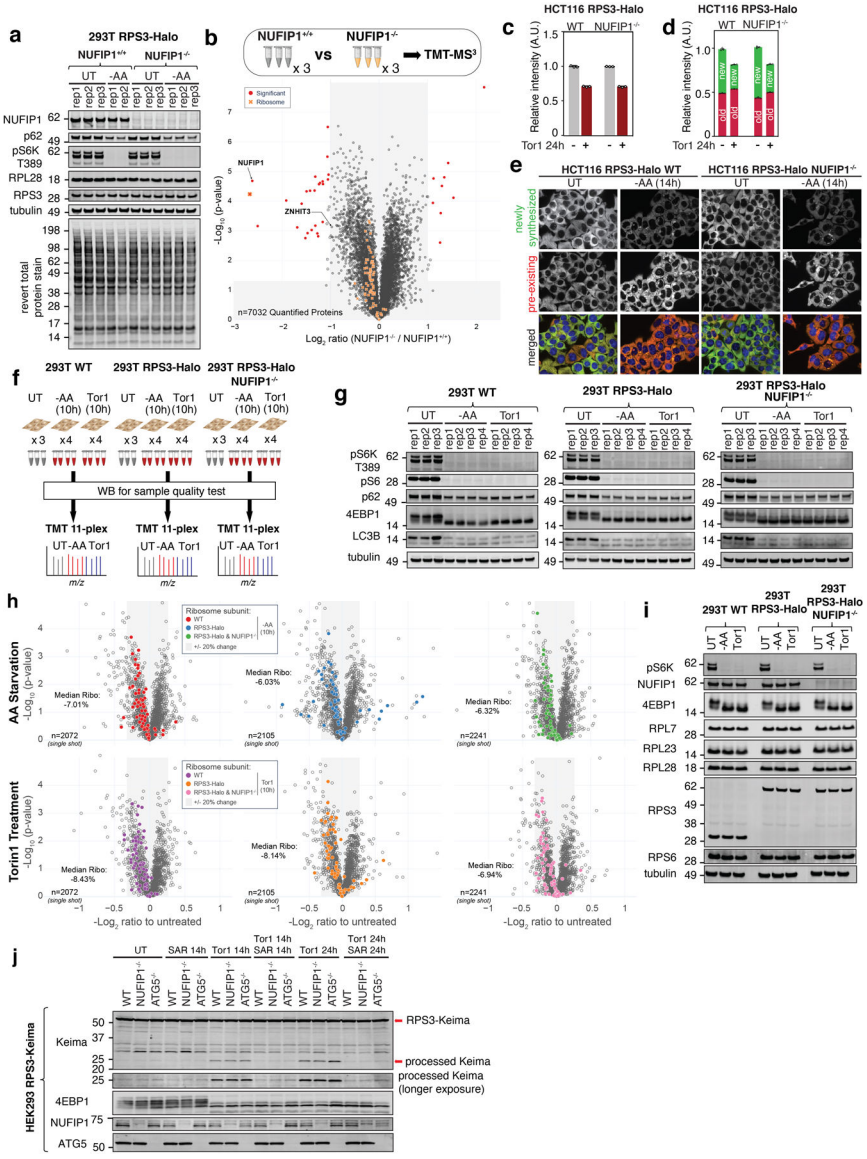

Extended Data Fig. 9 |. NUFIP1 deletion does not affect the ribosome inventory changes with nutrient stress.

a, Extracts from the 293T cells with or without NUFIP1 immunoblotted with the indicated antibodies after 10h of AA withdrawal, showing the same level of mTOR inhibition and r-proteins abundance regardless of the NUFIP1 deletion. Three biologically independent samples are blotted except two samples for NUFIP$^{+/+}$ -AA condition. **b**, Volcano plot ($-\text{Log}_{10}$ p-value versus Log_2 ratio (NUFIP1$^{-/-}$/WT)) of 293T cells with or without NUFIP1 deletion (n=7032 proteins). For two-sided Welch's t-test (adjusted for multiple comparison) parameters, individual p-values and q-values, see Supplementary Table 5. n=3 biologically independent samples per genotype. **c**, Normalized TMR signal in HCT116 RPS3-Halo NUFIP1$^{+/+}$ or $^{-/-}$ cells incubated with or without 200 nM Torin for 24h, followed by 1h TMR ligand treatment and flow-cytometry analysis. Mean of the triplicate data is plotted. Error bars represent ±SD. **d**, Average ratio of pre-existing to newly synthesized RPS3-Halo per cell with or without NUFIP1 plotted as a bar graph. Pre-existing Ribo-Halo proteins

were labeled with TMR-ligand (100 nM, 1h), followed by the addition of 50 nM Green-ligand. n=3 biologically independent samples. mean ±SD. **e**, Live-cell imaging of indicated Ribo-Halo cells with or without NUFIP1 labeled with TMR (for pre-existing r-proteins) and Green (for newly synthesized r-proteins) ligands with or without Tor1 (200 nM, 14h). Scale bar = 20 μm. **f**, Schematic description of the triple TMT-MS analysis of the whole cell lysates gathered from WT 293T or RPS3-Halo 293T cells with or without NUFIP1 after nutrient stress for 10h. **g**, Lysates of cells treated as in panel F were immunoblotted against the indicated antibodies for quality control, showing that mTOR activity was properly inhibited in all three cell types. **h**, Volcano plots ($-\text{Log}_{10}$ p-value versus Log_2 ratio Nutrient stress/Untreated) of the cells treated as in panel f (WT n=2072 proteins; RPS3-Halo n=2105 proteins; RPS3-Halo and NUFIP1$^{-/-}$ n=2241 proteins). Introducing HaloTag at the endogenous locus did not alter the mTOR inhibition nor ribosome abundance change after nutrient stress. Deletion of NUFIP1 did not show detectable difference either. For two-sided Welch's t-test (adjusted for multiple comparison) parameters, individual p-values and q-values, see Supplementary Table 5. n=3 (UT); 4 (-AA, Tor1) biologically independent samples per cell line. **i**, Immunoblotting of the cell lysates prepared as in panel F shows that introducing HaloTag at the endogenous locus did not alter the mTOR inhibition nor ribosome abundance change after nutrient stress. Deletion of NUFIP1 did not show detectable difference either, consistent with the TMT-MS analysis. **j**, Keima processing assay using the lysates from HEK293 RPS3-Keima WT or NUFIP$^{-/-}$ cells after the indicated nutrient stress. **k**, HEK293T WT and NUFIP1$^{-/-}$ cells were left untreated or treated with -AA medium for 3h. Cells were imaged by confocal microscopy after staining with α-NUFIP1 (top) and α-Lamp1 (bottom). Also see Supplementary Table 5. Experiments in e were repeated twice with similar results, and g,i,j were repeated three times independently with similar results. For gel source data, see Supplementary Fig. 1.

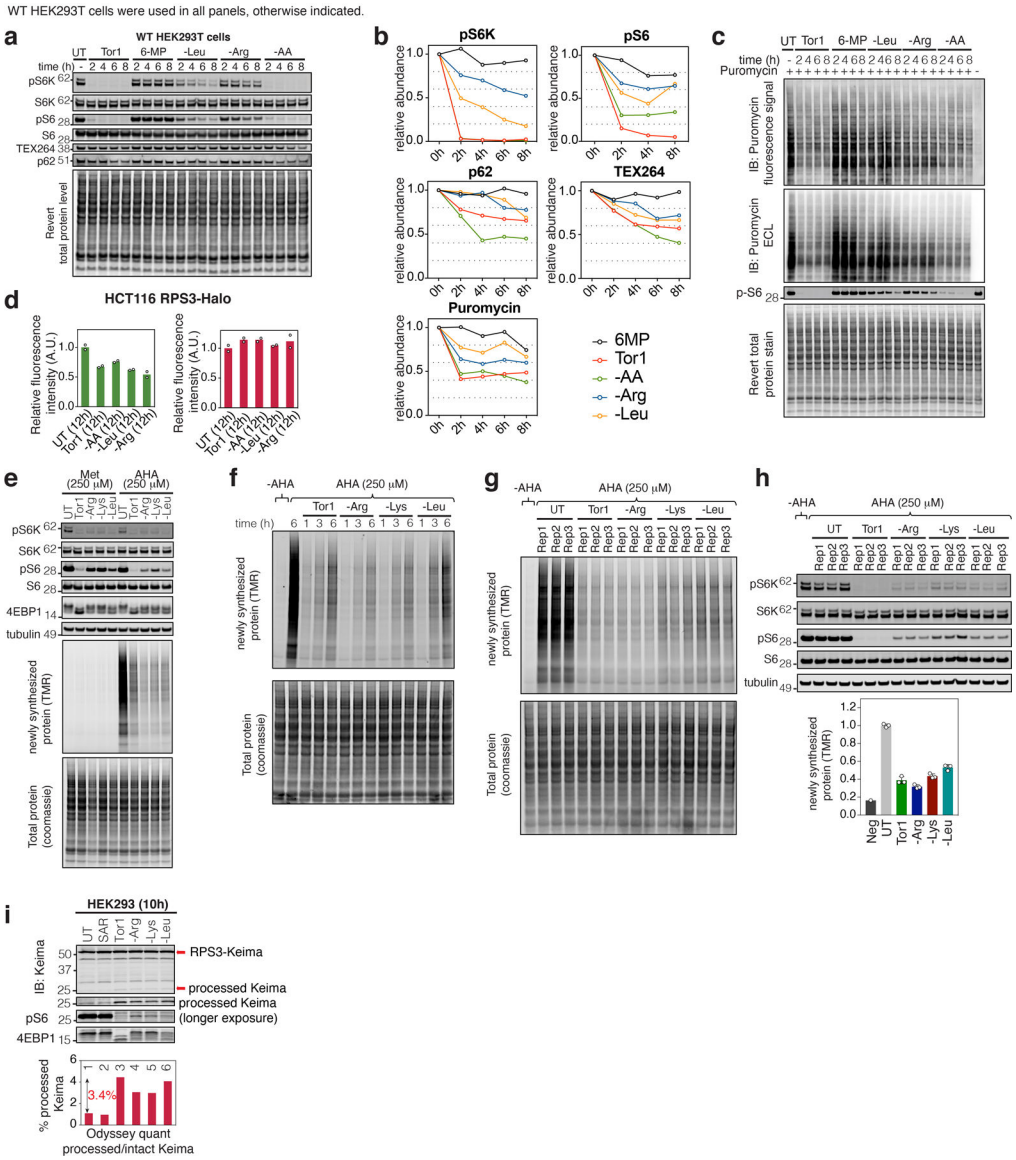

Extended Data Fig. 10 |. Systematic decoding of r-protein homeostasis in response to withdrawal of single AAs.

a, 293T cells were treated with either Tor1 or 6-MP or were incubated in media lacking Leu, Arg, or AAs for the indicated times and cell extracts subjected to immunoblotting with the indicated antibodies. **b,** Quantification of the WB data in panel a and c. **c,** Puromycin incorporation assay after treating 293T cells with the indicated medium and time course. Immunoblotting against anti-puromycin antibody was probed using either infra-red fluorophore labeled 2nd antibody coupled with Odyssey or Horseradish peroxidase labeled 2nd antibody coupled with ECL for comparison. **d,** Histograms show the quantification of the relative abundance of pre-existing (red) and newly synthesized (green) RPS3-Halo in Fig. 4b. mean, n=2. **e,** Cell extracted treated as indicated were analyzed for either mTOR inhibition or translatome using AHA incorporation assay coupled with TMR-alkyne click. **f**, Time-course protein synthesis assay was performed using AHA clicked with TMR-alkyne method after the indicated nutrient stress. **g,h,** Cells treated as in Fig. 4c were clicked with

TMR-alkyne and analyzed by in-gel fluorescence signal (panel g). Immunoblot assays using the indicated antibodies for quality control is shown in panel h (top), and relative TMR signal is plotted below. Centre data are mean ±SD. n=1, 3, 3, 3, 3 and 3 biologically independent samples, from left to right. **i,** Lysates from HEK293 RPS3-Keima cells after the indicated nutrient stress were immunoblotted against antibodies for Keima or mTOR substrates (top). Abundance ratio of the processed Keima to the intact Keima is plotted (bottom). Related to Fig. 4. Experiments in a,c,g,i were repeated three times independently with similar results, and e,f,i were performed once. For gel source data, see Supplementary Fig. 1.

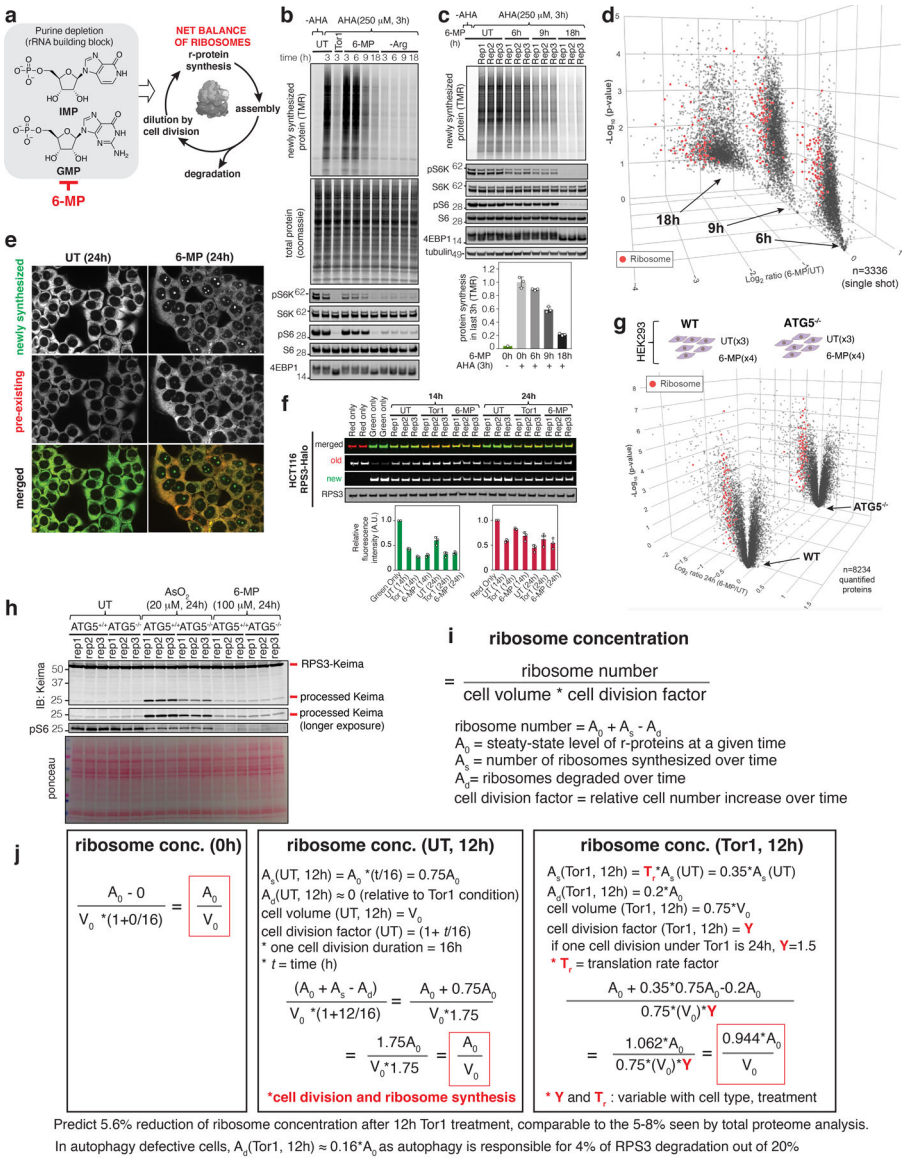

Extended Data Fig. 11 |. Systematic decoding of r-protein homeostasis in response to purine deficiency.

a, Schematic diagram indicating the points of intersection of nucleotides availability with net ribosome production. 6-MP is an inhibitor of purine biosynthesis and blocks production of rRNAs. **b,** 293T cells were treated with or without Tor1, 6-MP, or -Arg medium for the indicated time duration. Azidohomoalanine (AHA, 250 μM) was added 3 hours before collecting the cells. Lysates were either immunoblotted against the indicated antibodies for mTOR signaling inhibition (bottom) or processed for TMR-click reaction for in-gel fluorescence analysis (top). **c,** 293T cells treated with 6-MP for the indicated time points as well as AHA (for the last three hours) were analyzed for either mTOR inhibition (middle) or translatome using AHA incorporation assay coupled with TMR-alkyne click (top). Relative translation efficiency is plotted (bottom). Centre data are mean ±SD. n=1, 3, 3, 3 and 3 biologically independent samples, from left to right. **d,** 293T cells were incubated in the presence or absence of 6-MP for the indicated times, and AHA (250 μM) was added 3h

before collecting each lysate. The translatome was analyzed by biotinylation of AHA-labeled proteins followed by TMT-based proteomics. A volcano plot ($-Log_{10}$ p-value versus Log_2 6-MP/UT) showing the translatome and individual r-proteins (in red) at three time points. For two-sided Welch's t-test (adjusted for multiple comparison) parameters, individual p-values and q-values, see Supplementary Table 6. n=1 (Neg Ctrl); n=3 (UT, 9h); 2 (6h, 18h) biologically independent samples per cell line. **e,** Pre-existing RPS3 in HCT116 RPS3-Halo cells was labeled with TMR (red), washed and then incubated with media with green Halo ligand with or without 6-MP (24h). Live cells were imaged. **f,** HCT116 RPS3-Halo cells were subjected to 2-color labeling as in Fig. 2f. Cells were either left untreated or incubated with 6-MP prior to analysis of pre-existing and newly synthesized RSP3-Halo using in-gel fluorescence signal-based quantification. Histograms show the relative abundance of pre-existing (red) and newly synthesized (green) RPS3-Halo. Centre data are mean ±SD. n=2, 3, 3, 3, 3, 3 and 3 biologically independent samples, from left to right for both histograms. **g,** Total proteome analysis of 293T cells (with or without ATG5) was performed according to the scheme (top). Volcano plots ($-Log_{10}$ p-value versus Log_2 6-MP/UT) for all quantified proteins (n=8234 proteins), including individual r-proteins marked with a red dot, are shown at the bottom. For two-sided Welch's t-test (adjusted for multiple comparison) parameters, individual p-values and q-values, see Supplementary Table 6. n=3 (UT); 2 (6-MP) biologically independent samples per cell line. **h,** Keima processing assay using the lysates from HEK293 RPS3-Keima WT or $ATG5^{-/-}$ cells after 6-MP treatment (24h). Cells treated with arsenite was also blotted as a positive control, as it was previously reported to induce selective ribophagy. **i,j,** Analysis of ribosome concentration using biosynthetic, degradative and cell division information is shown as a simple equation in panel i. Panel j provides a change of ribosome concentration in response to nutrient stress using 0.2 as the degradation rate (derived from AHA-degradomics measurements), translation rates (T_r) of 0.35 derived from AHA-translatome analysis, and a cell cycle factor of 1.5 ($Y=1+t/24$, t=12h) derived from the proliferation assay. We find that the ribosome concentration upon 12h of Tor1 treatment $[0.944*A_0/V_0\}$ is comparable to the reduction in ribosomes we measured by total proteome analysis (reduction of ribosomes from ~5–8%). Summary of the systematic quantitative analysis of ribosome inventory during nutrient stress. Related to Fig. 4. Experiments in b were performed once, and e,h were repeated three times independently with similar results. For gel source data, see Supplementary Fig. 1.

Supplementary Material

Refer to Web version on PubMed Central for supplementary material.

ACKNOWLEDGMENTS

This work was supported by the National Institutes of Health (grants R37NS083524 and RO1GM095567 to J.W.H., and grant RO1GM132129 to J.A.P.). The authors acknowledge the Nikon Imaging Center (Harvard Medical School) for imaging assistance. We thank Scott Gruver and Marc Kirschner for providing MoxiGo II access and training.

REFERENCES

1. Thoreen CC et al. A unifying model for mTORC1-mediated regulation of mRNA translation. Nature 485, 109–113, doi:10.1038/nature11083 (2012). [PubMed: 22552098]

2. Saxton RA & Sabatini DM mTOR Signaling in Growth, Metabolism, and Disease. Cell 168, 960–976, doi:10.1016/j.cell.2017.02.004 (2017). [PubMed: 28283069]
3. Kraft C, Deplazes A, Sohrmann M & Peter M Mature ribosomes are selectively degraded upon starvation by an autophagy pathway requiring the Ubp3p/Bre5p ubiquitin protease. Nat Cell Biol 10, 602–610, doi:10.1038/ncb1723 (2008). [PubMed: 18391941]
4. Wyant GA et al. NUFIP1 is a ribosome receptor for starvation-induced ribophagy. Science 360, 751–758, doi:10.1126/science.aar2663 (2018). [PubMed: 29700228]
5. An H & Harper JW Systematic analysis of ribophagy in human cells reveals bystander flux during selective autophagy. Nat Cell Biol 20, 135–143, doi:10.1038/s41556-017-0007-x (2018). [PubMed: 29230017]
6. Wisniewski JR, Hein MY, Cox J & Mann MA "proteomic ruler" for protein copy number and concentration estimation without spike-in standards. Mol Cell Proteomics 13, 3497–3506, doi:10.1074/mcp.M113.037309 (2014). [PubMed: 25225357]
7. An H & Harper JW Ribosome Abundance Control Via the Ubiquitin-Proteasome System and Autophagy. J Mol Biol 432, 170–184, doi:10.1016/j.jmb.2019.06.001 (2020). [PubMed: 31195016]
8. Dieterich DC, Link AJ, Graumann J, Tirrell DA & Schuman EM Selective identification of newly synthesized proteins in mammalian cells using bioorthogonal noncanonical amino acid tagging (BONCAT). Proc Natl Acad Sci U S A 103, 9482–9487, doi:10.1073/pnas.0601637103 (2006). [PubMed: 16769897]
9. Sung MK et al. A conserved quality-control pathway that mediates degradation of unassembled ribosomal proteins. Elife 5:e19105, doi:10.7554/eLife.19105 (2016). [PubMed: 27552055]
10. Nguyen AT et al. UBE2O remodels the proteome during terminal erythroid differentiation. Science 357, doi:10.1126/science.aan0218 (2017).
11. Yanagitani K, Juszkiewicz S & Hegde RS UBE2O is a quality control factor for orphans of multiprotein complexes. Science 357, 472–475, doi:10.1126/science.aan0178 (2017). [PubMed: 28774922]
12. An H et al. TEX264 Is an Endoplasmic Reticulum-Resident ATG8-Interacting Protein Critical for ER Remodeling during Nutrient Stress. Mol Cell 74, 891–908 e810, doi:10.1016/j.molcel.2019.03.034 (2019). [PubMed: 31006537]
13. Miettinen TP & Bjorklund M Mevalonate Pathway Regulates Cell Size Homeostasis and Proteostasis through Autophagy. Cell Rep 13, 2610–2620, doi:10.1016/j.celrep.2015.11.045 (2015). [PubMed: 26686643]
14. Kiick KL, Saxon E, Tirrell DA & Bertozzi CR Incorporation of azides into recombinant proteins for chemoselective modification by the Staudinger ligation. Proc Natl Acad Sci U S A 99, 19–24, doi:10.1073/pnas.012583299 (2002). [PubMed: 11752401]
15. Thoreen CC The molecular basis of mTORC1-regulated translation. Biochem Soc Trans 45, 213–221, doi:10.1042/BST20160072 (2017). [PubMed: 28202675]
16. Kirkin V & Rogov VV A Diversity of Selective Autophagy Receptors Determines the Specificity of the Autophagy Pathway. Mol Cell, doi:10.1016/j.molcel.2019.09.005 (2019).
17. Zhao J, Zhai B, Gygi SP & Goldberg AL mTOR inhibition activates overall protein degradation by the ubiquitin proteasome system as well as by autophagy. Proc Natl Acad Sci U S A 112, 15790–15797, doi:10.1073/pnas.1521919112 (2015). [PubMed: 26669439]
18. Settembre C et al. TFEB links autophagy to lysosomal biogenesis. Science 332, 1429–1433, doi:10.1126/science.1204592 (2011). [PubMed: 21617040]
19. Liu Y et al. PWP1 Mediates Nutrient-Dependent Growth Control through Nucleolar Regulation of Ribosomal Gene Expression. Dev Cell 43, 240–252 e245, doi:10.1016/j.devcel.2017.09.022 (2017). [PubMed: 29065309]
20. de la Cruz J, Karbstein K & Woolford JL Jr. Functions of ribosomal proteins in assembly of eukaryotic ribosomes in vivo. Annu Rev Biochem 84, 93–129, doi:10.1146/annurev-biochem-060614-033917 (2015). [PubMed: 25706898]
21. Kakihara Y & Houry WA The R2TP complex: discovery and functions. Biochim Biophys Acta 1823, 101–107, doi:10.1016/j.bbamcr.2011.08.016 (2012). [PubMed: 21925213]

22. Shim MS, Nettesheim A, Hirt J & Liton PB The autophagic protein LC3 translocates to the nucleus and localizes in the nucleolus associated to NUFIP1 in response to cyclic mechanical stress. Autophagy, 1–14, doi:10.1080/15548627.2019.1662584 (2019).
23. Wolfson RL & Sabatini DM The Dawn of the Age of Amino Acid Sensors for the mTORC1 Pathway. Cell Metab 26, 301–309, doi:10.1016/j.cmet.2017.07.001 (2017). [PubMed: 28768171]
24. Darnell AM, Subramaniam AR & O'Shea EK Translational Control through Differential Ribosome Pausing during Amino Acid Limitation in Mammalian Cells. Mol Cell 71, 229–243 e211, doi:10.1016/j.molcel.2018.06.041 (2018). [PubMed: 30029003]
25. Hoxhaj G et al. The mTORC1 Signaling Network Senses Changes in Cellular Purine Nucleotide Levels. Cell Rep 21, 1331–1346, doi:10.1016/j.celrep.2017.10.029 (2017). [PubMed: 29091770]
26. Weinberg DE et al. Improved Ribosome-Footprint and mRNA Measurements Provide Insights into Dynamics and Regulation of Yeast Translation. Cell Rep 14, 1787–1799, doi:10.1016/j.celrep.2016.01.043 (2016). [PubMed: 26876183]
27. Chino H, Hatta T, Natsume T & Mizushima N Intrinsically Disordered Protein TEX264 Mediates ER-phagy. Mol Cell 74, 909–921 e906, doi:10.1016/j.molcel.2019.03.033 (2019). [PubMed: 31006538]
28. Poillet-Perez L et al. Autophagy maintains tumour growth through circulating arginine. Nature 563, 569–573, doi:10.1038/s41586-018-0697-7 (2018). [PubMed: 30429607]
29. Ran FA et al. Genome engineering using the CRISPR-Cas9 system. Nat Protoc 8, 2281–2308, doi:10.1038/nprot.2013.143 (2013). [PubMed: 24157548]
30. Ohana RF et al. HaloTag7: a genetically engineered tag that enhances bacterial expression of soluble proteins and improves protein purification. Protein Expr Purif 68, 110–120, doi:10.1016/j.pep.2009.05.010 (2009). [PubMed: 19464373]
31. Gu X et al. SAMTOR is an S-adenosylmethionine sensor for the mTORC1 pathway. Science 358, 813–818, doi:10.1126/science.aao3265 (2017). [PubMed: 29123071]
32. Suzuki K, Bose P, Leong-Quong RY, Fujita DJ & Riabowol K REAP: A two minute cell fractionation method. BMC Res Notes 3, 294, doi:10.1186/1756-0500-3-294 (2010). [PubMed: 21067583]
33. Paulo JA et al. Quantitative mass spectrometry-based multiplexing compares the abundance of 5000 S. cerevisiae proteins across 10 carbon sources. J Proteomics 148, 85–93, doi:10.1016/j.jprot.2016.07.005 (2016). [PubMed: 27432472]
34. McAlister GC et al. MultiNotch MS3 enables accurate, sensitive, and multiplexed detection of differential expression across cancer cell line proteomes. Anal Chem 86, 7150–7158, doi:10.1021/ac502040v (2014). [PubMed: 24927332]
35. Erickson BK et al. Active Instrument Engagement Combined with a Real-Time Database Search for Improved Performance of Sample Multiplexing Workflows. J Proteome Res 18, 1299–1306, doi:10.1021/acs.jproteome.8b00899 (2019). [PubMed: 30658528]
36. Schweppe DK et al. Full-Featured, Real-Time Database Searching Platform Enables Fast and Accurate Multiplexed Quantitative Proteomics. J Proteome Res, doi:10.1021/acs.jproteome.9b00860 (2020).
37. Schweppe DK et al. Characterization and Optimization of Multiplexed Quantitative Analyses Using High-Field Asymmetric-Waveform Ion Mobility Mass Spectrometry. Anal Chem 91, 4010–4016, doi:10.1021/acs.analchem.8b05399 (2019). [PubMed: 30672687]
38. Huttlin EL et al. A tissue-specific atlas of mouse protein phosphorylation and expression. Cell 143, 1174–1189, doi:10.1016/j.cell.2010.12.001 (2010). [PubMed: 21183079]
39. Eng JK, Jahan TA & Hoopmann MR Comet: an open-source MS/MS sequence database search tool. Proteomics 13, 22–24, doi:10.1002/pmic.201200439 (2013). [PubMed: 23148064]
40. Savitski MM, Wilhelm M, Hahne H, Kuster B & Bantscheff M A Scalable Approach for Protein False Discovery Rate Estimation in Large Proteomic Data Sets. Mol Cell Proteomics 14, 2394–2404, doi:10.1074/mcp.M114.046995 (2015). [PubMed: 25987413]
41. Beausoleil SA, Villen J, Gerber SA, Rush J & Gygi SP A probability-based approach for high-throughput protein phosphorylation analysis and site localization. Nat Biotechnol 24, 1285–1292, doi:10.1038/nbt1240 (2006). [PubMed: 16964243]

42. Tyanova S et al. The Perseus computational platform for comprehensive analysis of (prote)omics data. Nat Methods 13, 731–740, doi:10.1038/nmeth.3901 (2016). [PubMed: 27348712]

43. McShane E et al. Kinetic Analysis of Protein Stability Reveals Age-Dependent Degradation. Cell 167, 803–815 e821, doi:10.1016/j.cell.2016.09.015 (2016). [PubMed: 27720452]

44. Itzhak DN, Tyanova S, Cox J & Borner GH Global, quantitative and dynamic mapping of protein subcellular localization. Elife 5:e16950, doi:10.7554/eLife.16950 (2016). [PubMed: 27278775]

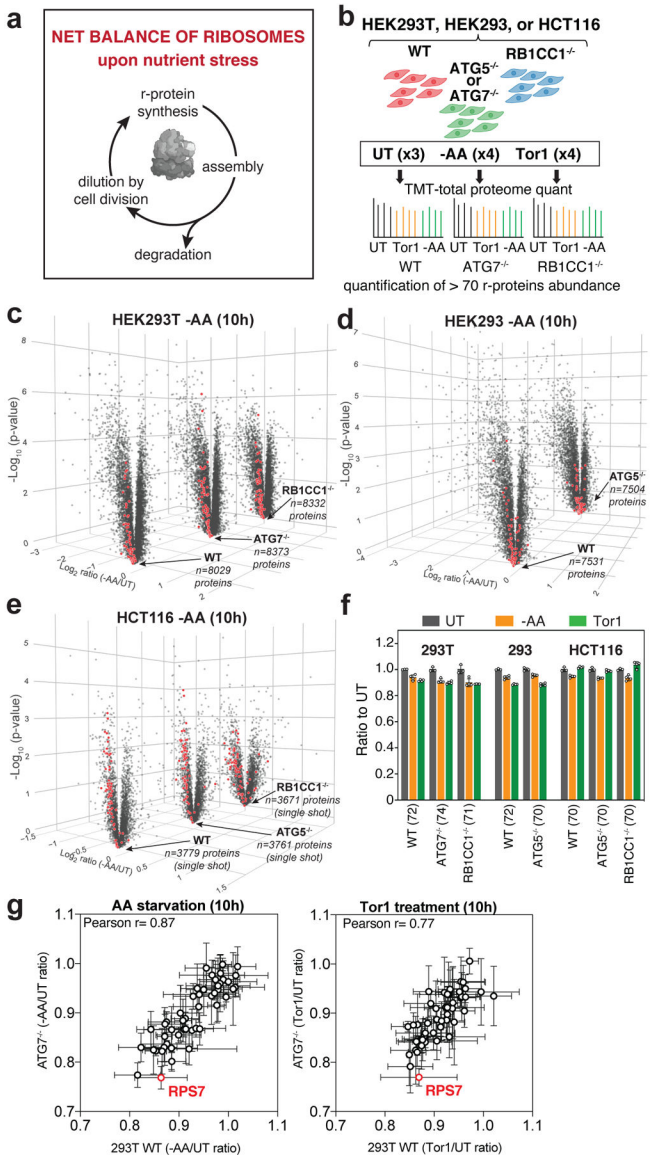

Fig. 1 |. Reduction in r-protein abundance during nutrient stress is largely autophagy independent.

a, Factors affecting net balance of ribosomes upon nutrient stress. **b**, 11-plex TMT pipeline to measure ribosome abundance upon nutrient stress +/− active autophagy. Normalized total cell extracts were processed for 8 11-plex TMT-MS^3 experiments. **c-e**, Volcano plots ($-\text{Log}_{10}$ p-value versus Log_2 ratio of -AA/UT) for 293T cells (n=8029 proteins), ATG7$^{-/-}$ (n=8373 proteins) or RB1CC1$^{-/-}$ (n=8332 proteins) (panel c), 293 cells (n=7531 proteins), ATG5$^{-/-}$ (n=7504 proteins) (panel d), or HCT116 cells (n=3779 proteins), ATG5$^{-/-}$ (n=3761 proteins) or RB1CC1$^{-/-}$ (n=3671 proteins) (panel e). n=3 (WT); 4 (-AA) biologically independent samples (c-e). For two-sided Welch's t-test (adjusted for multiple comparison) parameters, individual p-values and q-values, see Supplementary Table 1. **f**, Mean ratio value measured for ≥ 70 r-proteins treated as in panel b (n=72, 74, 71, 72, 70, 70, 70 and 70 r-proteins, from left to right). Error bars represent SD for n=3 (WT) or n=4 (-AA and Tor1) biologically independent samples. 293T data from[12]. **g**, Plots of relative abundance of

individual r-protein in 293T cells upon either 10h of AA withdrawal (left panel) or Tor1 treatment (right panel). 48 r-proteins with less than ±10% error range for every condition are plotted. Centre data are mean ±SD for n=3 (WT) or n=4 (-AA and Tor1) biologically independent samples.

See also Extended Data Fig. 1 and Supplementary Table 1.

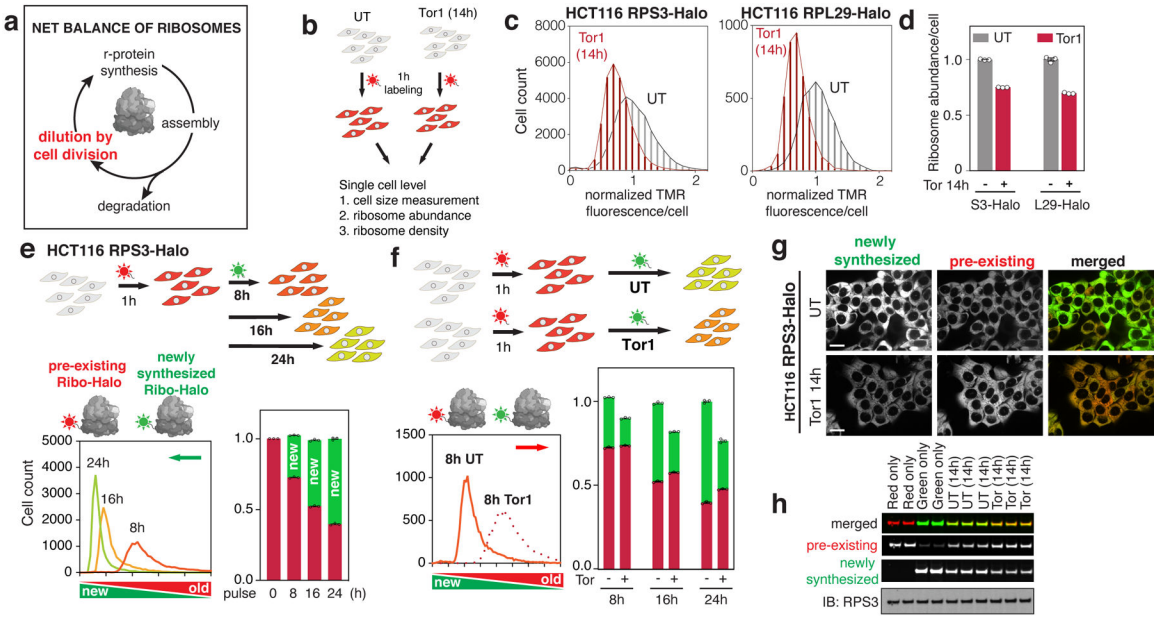

Fig. 2 |. r-protein density, synthesis, and dilution in single cells using Ribo-Halo.

a, Contribution of dilution by cell division to net ribosome balance upon nutrient stress. **b**, Measurement of r-protein concentration in single cells using one-color Halo labeling. **c**, Normalized TMR signal in RPS3-Halo (>3×10^5) and RPL29-Halo (>4×10^3) cells incubated +/− 200 nM Tor1 (14h), followed by 1h TMR ligand treatment and flow-cytometry. Representative of 3 independent experiments. **d**, Mean (± SD) of triplicate data from panel c is plotted. **e**, Pulse-chase Ribo-Halo in HCT116 cells. Pre-existing RPS3-Halo was labeled with TMR-ligand (1h) and newly synthesized RPS3-Halo was labeled with green R110-ligand for 8, 16 or 24h (top panel) prior to flow cytometry (frequency histogram, lower left panel, ~1.4×10^4 cells analyzed). Average from the triplicate experiments (bottom right panel). Error bars; SD. See METHODS for details. **f**, Scheme for two-color Ribo-Halo r-protein biogenesis and dilution labeling +/− Tor1 (top panel). Pre-existing RPS3-Halo was labeled with TMR-ligand (1h), and newly synthesized RPS3-Halo +/− Tor1 (200 nM) was labeled with green R110-ligand. The ratio of 561/620 to 488/550 plotted against cell populations (bottom left panel), and the mean values from triplicate experiments of 8h, 16h, and 24h pulse chase (bottom right panel) are shown. Error bars; SD. **g**, Imaging of pre-existing TMR-labeled RPS3-Halo and newly synthesized green R110-ligand labeled RPS3-Halo Green +/− Tor1 (200 nM, 14h). Scale bar = 20 μm. **h**, In-gel fluorescence of RPS3-Halo as in panel f. Gels were then transferred for immunoblotting with α-RPS3. Experiments shown in g-h were repeated >3 times with similar results. Full immunoblot is shown in Extended Data Fig. 11f. See also Extended Data Fig. 2, 3. For gel source data, see Supplementary Fig. 1.

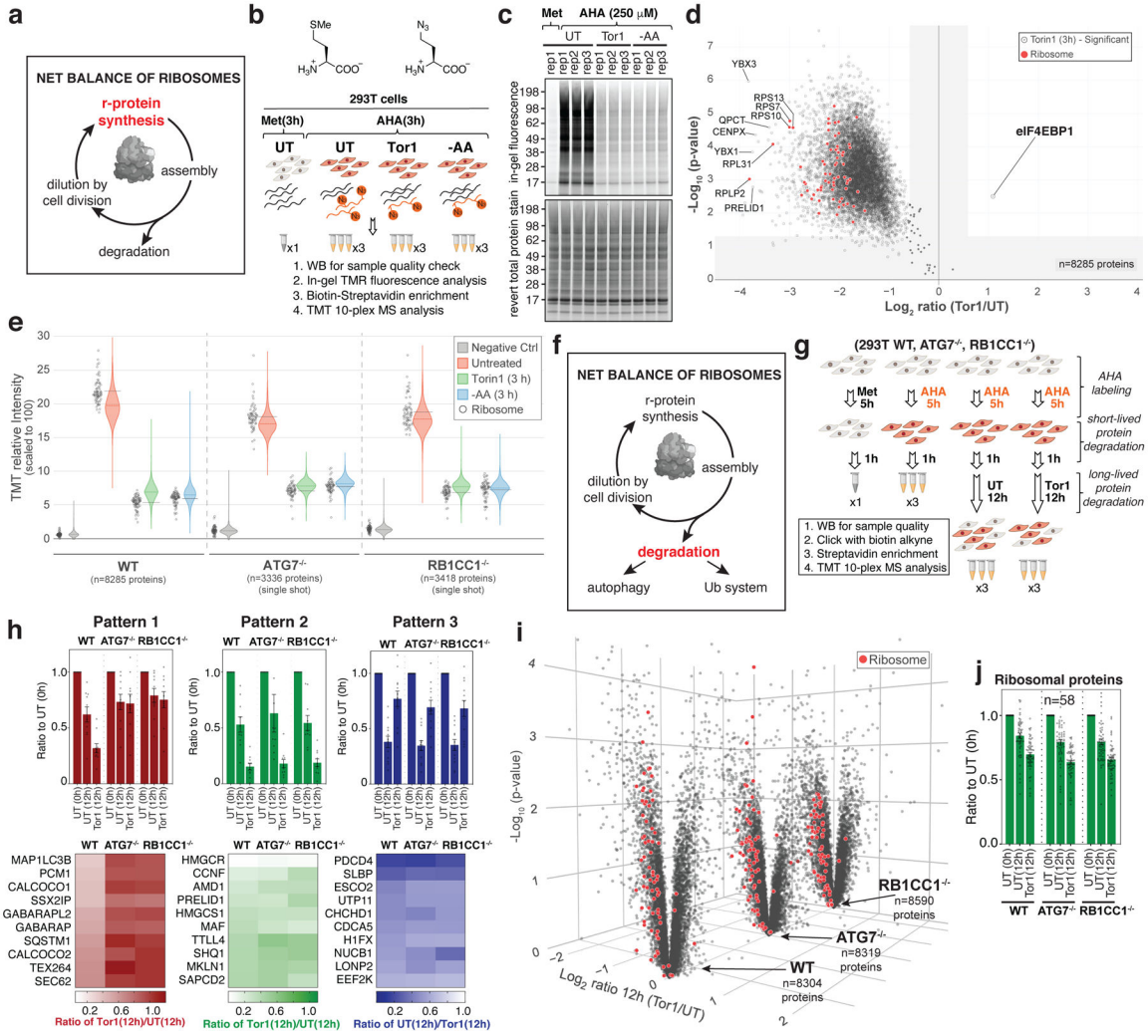

Fig. 3 |. Global translatome and degradome analysis during nutrient stress.

a, Contribution of r-protein synthesis to net ribosome balance upon nutrient stress. **b**, AHA-based translatomics to measure translational suppression during nutrient stress. **c**, Extracts from 293T cells +/− AA or Tor1 treatment in the presence of Met or AHA (250 μM, 3h each) were labeled with TMR and analyzed by in-gel fluorescence. n=3 biologically independent samples for UT, -AA, and Tor1, and n=1 for Met. **d**, 293T extracts (panel b) were clicked with biotin prior to streptavidin enrichment and proteomics. A plot of $-\mathrm{Log}_{10}$ p-value versus Log_2 ratio of Tor1/untreated for quantification (n=8285 proteins) is shown. n=3 biologically independent samples. For two-sided Welch's t-test (adjusted for multiple comparison) parameters, individual p- and q-values, see Supplementary Table 2. **e**, Violin plots for TMT intensity of newly synthesized proteins in WT, ATG7$^{-/-}$, or RB1CC1$^{-/-}$ 293T cells (n=8285, 3336, 3418 proteins, respectively). Black horizontal lines: median abundance of r-proteins (black circles). Colored horizontal dotted lines: median of all proteins. Violin plots represent the distribution and density of the whole dataset (Center-line: median; Limits: minima and maxima). **f**, Contribution of r-protein degradation to net ribosome balance upon nutrient stress. **g**, Schematic of degradomics analysis using AHA pulse

labeling (5h) to examine proteome turnover and autophagy dependence during mTOR inhibition (12h). Extracts were immunoblotted or clicked with biotin for TMT-proteomics. **h**, Pattern 1: accelerated degradation via autophagy. Pattern 2: accelerated degradation independent of autophagy. Pattern 3: stabilization independent of autophagy. n=10 proteins' average values from biological triplicate experiments; mean±SEM. **i**, Volcano plots ($-\text{Log}_{10}$ p-value versus Log_2 Tor1/UT 12h) for 293T WT, ATG7$^{-/-}$, and RB1CC1$^{-/-}$ cells (n=8304, 8319, 8590 proteins, respectively). r-proteins, red. n=3 biologically independent samples. For two-sided Welch's t-test (adjusted for multiple comparison) parameters, individual p- and q-values, see Supplementary Table 3. **j**, Average ratio for AHA-labeled r-proteins as in panel g. n=58 r-proteins (STDEV < 0.3 filter for every condition, n=3 biologically independent samples). mean±SEM. See also Extended Data Fig. 4–6 and Supplementary Table 2,3. For gel source data, see Supplementary Fig. 1.

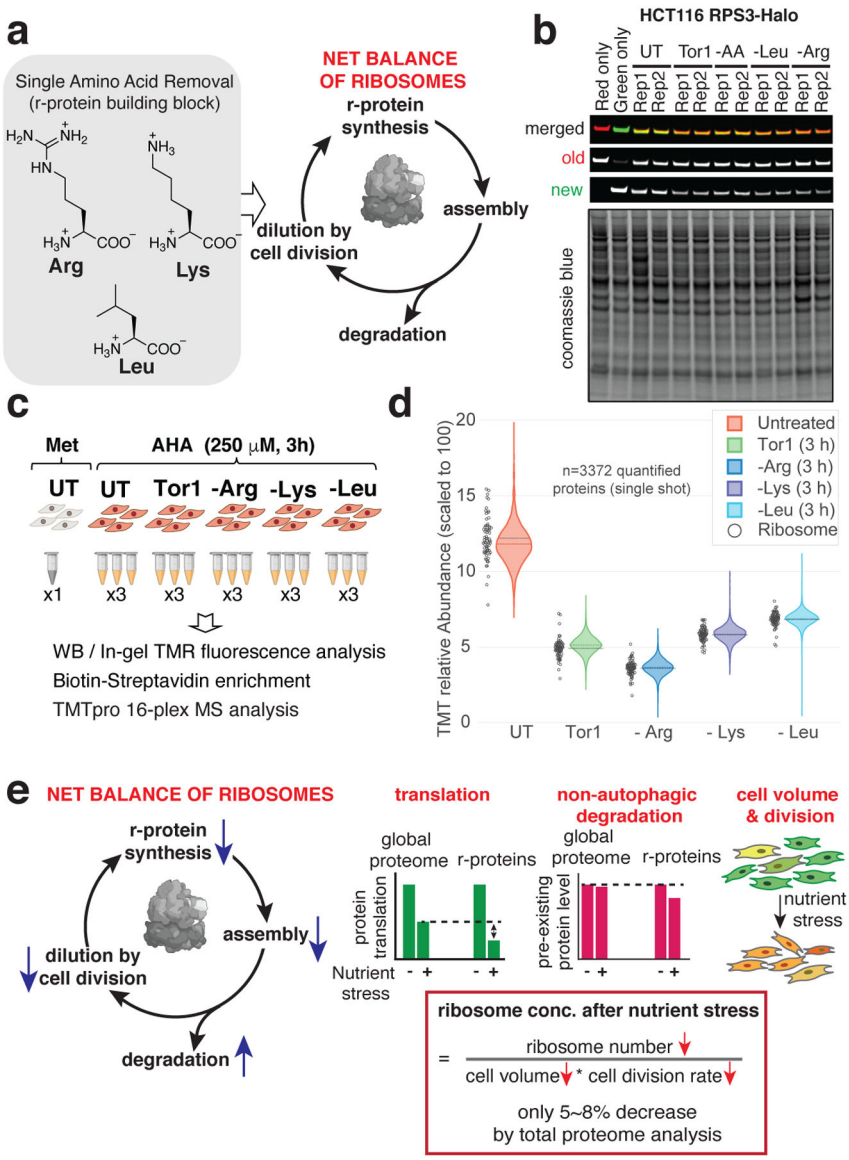

Fig. 4 |. Decoding of r-protein homeostasis in response to single AA perturbations.

a, Points of intersection of individual AAs with net ribosome production. **b**, HCT116 RPS3-Halo cells were either left untreated, subjected to AAs, Leu, or Arg withdrawal or incubated with Tor1 prior to analysis of pre-existing and newly synthesized RPS3-Halo as in Fig. 2f. For quantification of n=2 biologically independent experiments, see Extended Data Fig. 10d. **c**, Experimental workflow for AHA translatome analysis of 293T cells with or without the indicated AAs or with Tor1. **d**, Violin plots displaying the relative proteome translation rates and the effect of removal of indicated AAs or mTOR inhibition on the translation of individual r-proteins (black circles). The median abundance of r-proteins is indicated by the black horizontal lines and the median of all proteins is indicated by the colored horizontal dotted lines. The violin curves represent the distribution and density of the whole dataset (Center-line: median; Limits: minima and maxima). **e**, Ribosome homeostasis framework. Left panel: points of regulation, with blue arrows indicating the net effect of nutrient stress.

Right panel compares the effect of nutrient stress on global proteome and r-protein translation and degradation, primarily through non-autophagic mechanisms, and the effect of nutrient stress on r-protein dilution via cell division. Ribosome concentration upon nutrient stress in a population of cells will reflect a decrease in r-protein number through translational and degradative mechanisms corrected for by changes in cell volume and cell division. See also Extended Data Fig. 10 and Supplementary Table 6. For gel source data, see Supplementary Fig. 1.